TOXICOLOGY AND APPLIED PHARMACOLOGY **152,** 211–231 (1998)
ARTICLE NO. TO988492

Application of a Hybrid Computational Fluid Dynamics and Physiologically Based Inhalation Model for Interspecies Dosimetry Extrapolation of Acidic Vapors in the Upper Airways

Clay B. Frederick,*[,1] Michele L. Bush,† Larry G. Lomax,* Kurt A. Black,* Lavorgie Finch,* Julia S. Kimbell,‡ Kevin T. Morgan,‡ Ravi P. Subramaniam,‡ John B. Morris,§ and James S. Ultman†

*Toxicology Department, Rohm and Haas Company, Spring House, Pennsylvania 19477; †Physiological Transport Studies Laboratory, Department of Chemical Engineering, The Pennsylvania State University, University Park, Pennsylvania 16802-4400; ‡Chemical Industry Institute of Toxicology, Research Triangle Park, North Carolina 27709; and §Toxicology Program, School of Pharmacy, University of Connecticut, Storrs, Connecticut 06269-2092

Received February 11, 1998; accepted May 26, 1998

Application of a Hybrid Computational Fluid Dynamics and Physiologically Based Inhalation Model for Interspecies Dosimetry Extrapolation of Acidic Vapors in the Upper Airways. Frederick, C. B., Bush, M. L., Lomax, L. G., Black, K. A., Finch, L., Kimbell, J. S., Morgan, K. T., Subramaniam, R. P., Morris, J. B., and Ultman, J. S. (1998). *Toxicol. Appl. Pharmacol.* **152, 211–231.**

This study provides a scientific basis for interspecies extrapolation of nasal olfactory irritants from rodents to humans. By using a series of short-term *in vivo* **studies,** *in vitro* **studies with nasal explants, and computer modeling, regional nasal tissue dose estimates were made and comparisons of tissue doses between species were conducted. To make these comparisons, this study assumes that human and rodent olfactory epithelium have similar susceptibility to the cytotoxic effects of organic acids based on similar histological structure and common mode of action considerations. Interspecies differences in susceptibility to the toxic effects of acidic vapors are therefore assumed to be driven primarily by differences in nasal tissue concentrations that result from regional differences in nasal air flow patterns relative to the species-specific distribution of olfactory epithelium in the nasal cavity. The acute, subchronic, and** *in vitro* **studies have demonstrated that the nasal olfactory epithelium is the most sensitive tissue to the effects of inhalation exposure to organic acids and that the sustentacular cells are the most sensitive cell type of this epithelium. A hybrid computational fluid dynamics (CFD) and physiologically based pharmacokinetic (PBPK) dosimetry model was constructed to estimate the regional tissue dose of organic acids in the rodent and human nasal cavity. The CFD–PBPK model simulations indicate that the olfactory epithelium of the human nasal cavity is exposed to two- to threefold lower tissue concentrations of a representative inhaled organic acid vapor, acrylic acid, than the olfactory epithelium of the rodent nasal cavity when the exposure conditions are the same. The magnitude of this difference varies somewhat with the specific exposure scenario that is simulated. The increased olfactory tissue dose in rats relative to humans may be attributed to the large rodent olfactory surface area (greater than 50% of the nasal cavity) and its highly susceptible location (particularly, a projection of olfactory epithelium extending anteriorly in the dorsal meatus region). In contrast, human olfactory epithelium occupies a much smaller surface area (less than 5% of the nasal cavity), and it is in a much less accessible dorsal posterior location. In addition, CFD simulations indicate that human olfactory epithelium is poorly ventilated relative to rodent olfactory epithelium. These studies suggest that the human olfactory epithelium is protected from irritating acidic vapors significantly better than rat olfactory epithelium due to substantive differences in nasal anatomy and nasal air flow. Furthermore, the general structure of the hybrid CFD–PBPK model used for this study appears to be useful for target tissue dosimetry and interspecies dose comparisons for a wide range of inhaled vapors.**

A variety of volatile compounds induce toxic effects in the rodent nasal cavity following inhalation exposure. Interestingly, the distribution of histopathological lesions is often localized in specific regions or is limited to one epithelial type (reviewed in Morgan and Monticello, 1990; Mery *et al.,* 1994). The regional distribution of toxic effects from inhaled vapors has been correlated with the nasal air flow patterns, i.e., regions of high air flow tend to exhibit a higher incidence and greater severity of toxic effects than regions of low air flow (Morgan and Monticello, 1990; Kimbell *et al.,* 1993, 1997; Mery *et al.,* 1994). This pattern of localized toxicity emphasizes the importance of local tissue dose for interspecies extrapolation and risk assessment. Furthermore, observation of toxic effects localized in specific epithelial types (variable depending on the inhaled vapor) emphasizes the importance of chemical-specific differences in mode of action and tissue susceptibility.

Typically, high vapor concentrations of irritating organic acids and esters preferentially induce cytotoxicity of the olfactory epithelium in the nasal cavity (e.g. Keenan *et al.,* 1990;

[1] To whom correspondence should be addressed. Fax: (215) 619-1621. E-mail: cfrederick@rohmhaas.com.

0041-008X/98 $25.00

Trela and Bogdanffy, 1991; Miller *et al.*, 1981, 1985). Respiratory epithelium in the rodent nasal cavity is typically much less sensitive to inhaled organic acids and esters and generally does not exhibit histopathological lesions, although high inhaled concentrations of strong acids have been demonstrated to induce cytotoxicity in this region also (e.g., formic acid; National Toxicology Program, 1992). The biochemical basis for the olfactory toxicity has not been fully explored, but the pathogenesis is apparently based on the high susceptibility of a particular cell type, olfactory sustentacular cells, to acids and esters (e.g., Lee *et al.*, 1992; Trela *et al.*, 1992).

There is a wide interspecies variability in nasal anatomy (Gross and Morgan, 1992), in the amount of olfactory epithelium relative to respiratory epithelium in the nasal cavity (DeSesso, 1993) and in the localization of the olfactory epithelium relative to the main nasal air streams (Morgan *et al.*, 1991; Hahn *et al.*, 1993; Keyhani *et al.*, 1995). This provides a substantive problem for interspecies extrapolation and risk assessment. The regulatory significance of the problem is emphasized by the frequent use of histopathology in the rodent nasal cavity to establish inhalation exposure limits for industrial workers and the public, e.g., many of the Environmental Protection Agency's (EPA) reference concentrations (RfCs) for vapors are based on rodent nasal histopathology.

This study evaluated the acute nasal toxicity of an organic acid, acrylic acid, that is primarily used to make a variety of aqueous emulsion polymers. Additional histopathological dose–response data were collected *in vitro* using explants of nasal epithelium cultured with acrylic acid solutions. The *in vivo* and *in vitro* histopathological dose–response data, partitioning information, and total nasal deposition data from additional *in vivo* studies were correlated with the output of an inhalation dosimetry model. The dosimetry model incorporated the anatomy, air flow patterns, and flux of inhaled vapor into the walls of a model of either the rat or human nasal cavity obtained as output from computational fluid dynamics (CFD) simulations. This port of entry was linked to a systemic compartmental physiologically based pharmacokinetic (PBPK) model for each species. An important feature of this hybrid CFD-PBPK dosimetry model was the capacity to estimate target tissue dose of inhaled vapors in specific regions of the nasal cavity for a wide range of exposure scenarios. These dose estimates facilitated quantitative comparisons of interspecies differences in the deposition of the absorbed vapors in the nasal epithelium and systemic tissues. The specific design criteria for the construction and evaluation of the CFD–PBPK model were based on the production of a generally useful dosimetry model that would comprehensively describe the available experimental data that relate to regional and whole-nose nasal tissue dose (e.g., decreasing fractional deposition of a vapor in the overall nasal cavity with increasing inhalation flow rate, changes in overall nasal deposition of a vapor by modulating the rate of metabolism of the vapor in the nasal cavity, changes in the rate of nasal uptake of an inhaled vapor as a function of time in extended exposure scenarios as the arterial blood concentration increases due to systemic loading of the vapor, etc.) (Frederick *et al.*, 1994). Notably, the CFD–PBPK model incorporates a unique interface to link the data from CFD simulations of air flow in the upper respiratory tract (of potentially any species or any number of individuals) with a compartmental PBPK model with the capacity to describe systemic distribution, metabolism, and excretion as well as systemic target tissue dose. The general model structure appears to be useful for tissue dose estimates and interspecies extrapolation for a wide range of inhaled vapors. To provide a basic dataset to evaluate the CFD-PBPK model structure, the model was initially used to evaluate the rodent nasal deposition of several poorly metabolized vapors. To further explore the relationship of regional nasal tissue dose and histopathology, the model was used to evaluate the olfactory tissue dose of an inhaled organic acid in both rats and humans under the same simulated exposure conditions. The data from these studies provide a scientific basis for tissue dose comparisons, interspecies extrapolation, and risk assessment.

MATERIALS AND METHODS

Chemicals. The glacial acrylic acid (CAS 70-10-7) used for these studies was flocculent grade containing 200 ppm MEHQ (Rohm and Haas Co., Deer Park, TX) with a purity of 99.9 $\pm$ 0.1% by gas chromatography.

Acute inhalation exposure of rats. Female F344/N rats (approximately 60 to 75 days old upon arrival; weight range of 160 to 175 g 1 day prior to exposure) were obtained from Charles River Laboratories (Wilmington, MA). Food and filtered tap water were supplied *ad libitum*, except during inhalation exposure, when food and water were withheld. The animals were administered a single, whole-body inhalation exposure of 0 or 75 ppm acrylic acid vapor for 3 or 6 h in a 240-liter exposure chamber. The exposure atmosphere was generated by passing compressed air over the surface of acrylic acid liquid maintained at approximately 40°C in a 250-ml glass jar. The vapor was diluted with conditioned laboratory air to the appropriate concentration (monitored by a Foxboro MIRAN 1A infrared gas analyzer that had been calibrated by gas chromatography of impinger samples) and entered the top of the exposure chamber. The animals were housed in individual cages during the exposure period.

Immediately following exposure, the animals were removed from the inhalation apparatus, anesthetized with sodium pentobarbital, and then killed by exsanguination by cutting the abdominal aorta. The nasal cavity was infused with 10% neutral-buffered formalin via the pharyngeal duct, the head was then immersed and fixed in formalin, decalcified, and sectioned transversely at Levels I through IV (Young, 1981). The tissue sections were processed, microtomed at 4 to 6 μm, stained with hematoxylin and eosin, and evaluated for histopathology. Lesions were characterized according to the scheme used previously (Lomax *et al.*, 1994), and their locations were mapped according to the scheme described by Mery *et al.* (1994). A composite regional map was also constructed for each group. The recording of lesions was designed to qualitatively assess the extent, nasal region affected, and type of histologic lesions within the nasal cavity.

In vitro incubation of nasal explants with acrylic acid. Nasal septa were carefully collected from female F344/N rats (weight range of 150 to 225 g) and incubated for 2 h in DMEM/F12 media supplemented with antibiotics (penicillin, streptomycin, and nystatin), insulin, transferrin, selenium, hydrocortisone, and epidermal growth factor under an atmosphere of 95% O_2 and 5% CO_2 at 37°C. For treated tissues, 0.0 to 6.0 mM acrylic acid was added to the

medium prior to the addition of the tissues, and the treated medium was adjusted to pH 7.3 with 1 N sodium hydroxide. After incubation, the tissues were fixed with formalin, decalcified, imbedded in glycol methacrylate, microtomed at 2 to 3 μm, stained with hematoxylin and eosin, and evaluated for histopathology.

Partition coefficients. Liquid:air partitioning of acrylic acid vapor was evaluated as described by Gargas *et al.* (1989) for saline (unbuffered), phosphate buffer, rat blood, and rat inguinal fat. Each solution was evaluated under the following three conditions: unbuffered, at pH 2.0 with phosphate buffer, and at pH 7.4 with phosphate buffer. In addition, liquid:air partitioning with water (unbuffered), DMEM/F12 tissue culture media, octanol, and olive oil were evaluated. Liquid:air partitioning of acetic acid was evaluated similarly with unbuffered saline and phosphate buffer at pH 2.0 and 7.4.

Simulations of nasal air flow and estimation of gas phase mass transport coefficients with CFD. Simulations were conducted with CFD software (FIDAP from Fluent, Lebanon, NH) to evaluate regional air flow and gas phase mass transport coefficients for rats and humans. Steady-state simulations were conducted using a three-dimensional computer model ("mesh") of both the anterior rat nasal cavity (Kimbell *et al.*, 1993, 1997; Godo *et al.*, 1995) and the human nasal cavity (Subramaniam *et al.*, 1998). Effectively, these simulations estimated regional air-phase delivery of the vapor to the mucus lining the nasal airway. The simulations were conducted at inspiratory flow rates of 100, 300, and 500 ml/min (rat) and 11,400 and 18,900 ml/min (human). The CFD simulations were restricted to steady inspiratory flow conditions, and only laminar flows were considered in modeling transport. The importance of unsteady effects has been characterized as negligible by Subramaniam *et al.* (1998) and Keyhani *et al.* (1995). Thermal convection effects have also been ignored based on the analysis by Keyhani *et al.* (1995) that indicated that they were negligible. The nasal walls have been assumed to be rigid and hairless, and dynamic changes in air flow due to the occlusive effects of nasal cycling have been ignored. Simulations were conducted with the computer model of the human nasal cavity with gas phase diffusivities of 0.05, 0.1, and 0.15 cm^2/s. These studies indicated that the flux of the vapor to the wall of the nasal cavity varies as a near-linear function of the gas phase diffusivity over this limited diffusivity range. For many of the CFD simulations, a gas phase diffusivity of 0.15 cm^2/s was used and the gas phase mass transport coefficient was scaled proportionally for vapors with differing diffusivities (0.6 for acrylic acid). Experimental determinations of air phase diffusivity of a wide variety of representative organic vapors in the 30 to 150 MW range have ranged from 0.2 to 0.07 cm^2/s (Cussler, 1997). Interspecies dose comparisons for acrylic acid were conducted with gas phase mass transport coefficients derived from CFD simulations for the human nasal cavity that were conducted with a gas phase diffusivity of 0.1 cm^2/s and with proportional scaling of the CFD data for the rat nasal cavity. As discussed by Bush *et al.* (1998), deposition of vapors in the rat nasal cavity is relatively insensitive to significant variation in the gas phase mass transport coefficients.

The inhalation flow rates used for the CFD exercises were chosen to simulate ventilation characteristic of resting conditions to light physical activity for each species (ICRP, 1975; Kimbell *et al.*, 1993, 1997; Subramaniam *et al.*, 1998). The "C = 0 boundary conditions" (the assumption that the concentration of the vapor in the nasal airway lining is always zero) used for each mesh in these studies simulates a nasal epithelium with an infinitely large mucus:air partition coefficient and/or an infinitely fast rate of reaction of the vapor molecules upon collision with the mucus layer (i.e., the CFD simulations allowed no "back pressure" or desorption to limit wall uptake). Effectively, this assumption decouples the tissue resistance from the gas phase resistance. With some modifications reported in the Appendix, the methods described by Bush *et al.* (1998) were used to calculate the regional gas phase mass transport coefficients for each flow rate. The finite element calculations used for the CFD simulations of nasal air flow are subject to numerical errors in the mass balance. In the case of the CFD simulations of the human nasal cavity, the mass balance error for the overall uptake was up to 8%. Assuming as a first approximation that the percentage error is uniformly distributed within the nasal cavity, then the error in a given compartment is proportional to its diffusion surface.

Structure of physiologically based inhalation model. A whole-body compartmental physiologically based inhalation model was constructed with ACSL for Windows (Mitchell and Gauthier Associates, Concord, MA). This model included a nasal cavity as a port of entry for inhaled acidic vapors that was based on a compartmental rat nasal model for nonmetabolized and poorly metabolized vapors (Bush *et al.*, 1998). A critical component of the nasal CFD–PBPK model that was necessary for interspecies extrapolation was a modular description of nasal air flow and the calculation of compartmental gas phase mass transfer coefficients in both the rodent nasal cavity (Kimbell *et al.*, 1993, 1997) and human nasal cavity (Subramaniam *et al.*, 1998) using data from CFD simulations (methods described above). The liquid phase of the model of Bush *et al.* (1998) was modified to include the effect of buffering capacity on the ionization of the acid in the mucus, diffusion of both the ionized form of the acid (presumably, primarily the salt, sodium acrylate) and the nonionized species, liquid:air partition coefficients, tissue:blood partition coefficients (Black and Finch, 1995), and metabolism of acrylic acid (Black and Finch, 1995). The Appendix describes methods used to incorporate the results from the CFD simulations and lists the additional model parameters (and their derivation) used to modify the model of Bush *et al.* (1998) for acrylic acid. Cyclic flow simulations of breathing were conducted by alternately reversing air flow to simulate inhaling and exhaling. Exhalation was modeled by reversing the air flow from the CFD simulations of unidirectional flow of inhaled air. More refined analyses in future models could easily incorporate changes in air flow patterns and gas phase mass transfer between inhalation and exhalation.

Conceptually, the model could be constructed with any number of compartments. For this study, the interspecies comparisons were conducted with a relatively simple anatomically based compartmental model (Figs. 1 and 2) consisting of all inhaled air flowing across the nasal vestibule, a dorsal medial airstream flowing over respiratory epithelium and then olfactory epithelium, and a second composite ventral and lateral air stream flowing over the remaining respiratory epithelium in the nasal cavity (divided into anterior and posterior compartments). All air from the nasal cavity then passes over a nasopharynx compartment before entering a composite lower respiratory tract compartment (which could be further subdivided into additional compartments for regional dose estimates, if necessary). The large olfactory region of rodents was divided into two compartments (Figs. 1 and 2), a small dorsal anterior compartment (13% of the olfactory epithelium and 7% of the total nasal surface area) and a large compartment representing the remaining olfactory epithelium on the septum and ethmoid turbinates (data from nasal CFD mesh and Gross *et al.*, 1982). The human nasal cavity (Figs. 1 and 2) does not have an anatomical equivalent for the rat ethmoid turbinates that are covered primarily with olfactory epithelium; consequently, the small human olfactory epithelium was described by one compartment comprising approximately 4% of the total nasal surface area (Lang, 1989).

The diffusion path from the nasal lumen to the blood exchange region (liquid phase) of each compartment was divided into a 10- to 20-μm-thick mucus layer and underlying epithelial cell layers that were 15- to 20-μm thick (Fig. 2B; two cell layers for respiratory epithelium and four cell layers for the thicker olfactory epithelium). The thicknesses of the rat respiratory and olfactory epithelia were determined from photomicrographs of each tissue relative to photomicrographs of a calibrated micrometer at the same magnification. The thicknesses of the rat nasal epithelia are consistent with similar measurements of human nasal epithelia (Lang, 1989), therefore the same epithelial structure was used to model each species. This layered description of the epithelium was based upon the approach used by Morris *et al.* (1993) to approximate the concentration gradient across nasal tissue from the mucus layer to the vascularized region under the basal lamina, which serves to remove nonmetabolized vapors in the venous blood. In addition, the bodies of the olfactory sustentacular cells (the cells that are most sensitive to the toxic effects of organic acids) line the nasal lumen immediately under the mucus layer. Therefore, the apical

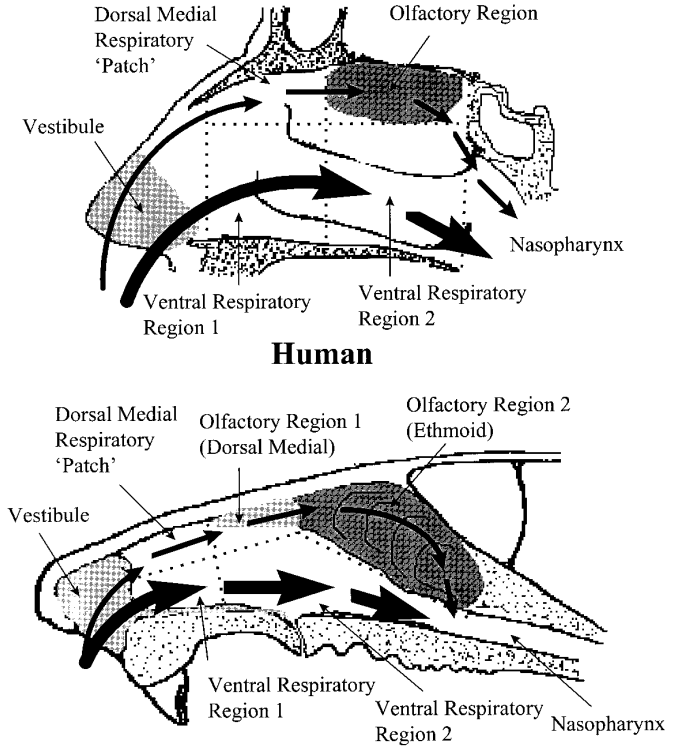

FIG. 1. Rat and human nasal anatomy divided into compartments corresponding to the epithelium lining the lumen. The squamous epithelium lining the vestibule of the human nasal cavity is primarily anterior to the nasal valve. The human nasal cavity lacks a region lined with olfactory tissue that is comparable to the rat ethmoid turbinates. The figure of the human nasal cavity was modified from Lang (1989) and the figure of the rat nasal cavity was modified from Miller *et al.* (1993). The arrows designate the air flow streams described by the CFD–PBPK, which are described in more detail by Kimbell *et al.* (1993, 1997) for the rat nasal cavity and by Keyhani *et al.* (1995) and Subramaniam *et al.* (1998) for the human nasal cavity.

epithelial layer simulated by the model in the olfactory region effectively corresponds to the target cell population for toxic effects.

RESULTS

Acute Inhalation Exposure of Rats to Acrylic Acid

The olfactory epithelium of the nasal cavity was identified as the primary target tissue in rats inhaling 75 ppm acrylic acid vapor for either 3 or 6 h (Table 1). Control animals exhibited no detectable lesions in the nasal cavity, nor were lesions present in the squamous epithelium of rats exposed to acrylic acid. Lesions were confined to the dorsal aspects of the nasal cavity, in particular the dorsal meatus, the dorsomedial aspects of the nasoturbinate, and ethmoturbinate 3 (Fig. 3). The lesions were small and most of the olfactory and respiratory epithelium in the treated animals was normal histologically. However, the extent of the lesions increased as the exposure time was increased from 3 to 6 h.

Olfactory epithelial cell degeneration was accompanied by sustentacular cell necrosis (Fig. 4). These lesions were observed in all four sections of the nasal cavity at both 3 and 6 h of exposure, although the area of mucosa affected and the incidence of affected animals was greater in the anterior three sections. Limited regions of respiratory epithelial degeneration and desquamation were present in Section I in animals exposed for 6 h (Table 1). Lesions of the respiratory epithelium were not observed in Sections II and III. Section IV did not contain respiratory epithelium.

In Vitro Incubation of Nasal Explants with Acrylic Acid

Short-term organ culture of nasal explants with media containing acrylic acid resulted in histopathological lesions very similar to those observed *in vivo* (Fig. 5; Table 2). Since the tissue culture medium has a liquid:air partition coefficient for acrylic acid that is very similar to that of blood (Table 3) and the acrylic acid epithelial tissue:blood partition coefficients are approximately one (Black and Finch, 1995), it may be assumed that the concentration of acrylic acid in the tissue explants is approximately the same as the medium (note that metabolism of acrylic acid by epithelial tissues is not fast enough to generate a significant concentration gradient; Black and Finch, 1995). This would suggest that the steady-state tissue concentration of acrylic acid required to induce sustentacular cell cytotoxicity and subsequent loss of neuronal cells must be at least 0.5 mM with actual loss of sustentacular and neuronal cells observed *in vitro* in the 3 to 6 mM concentration range. An acrylic acid concentration of 0.4 mM in the medium (and consequently in the tissue) is a no-observed-adverse-effect level (NOAEL) in this assay. No cytotoxicity was observed in the respiratory epithelium, suggesting that the acrylic acid concentration required to induce cytotoxicity in respiratory epithelium in this assay is in excess of 6 mM.

Partition Coefficients for Acrylic Acid

The partitioning of acrylic acid between air and liquid phases was evaluated with unbuffered, neutral, and acidic liquid phases (Table 3). The data indicate a strong preference for acrylic acid partitioning into the aqueous phase, regardless of blood pH (i.e., acid dissociation contributes to the preference for the liquid phase, but it is not the determining factor), which is consistent with the highly polar structure of this small organic acid. The partition coefficients of all of the tissues, saline, and oil at neutral pH are similar to that of the tissue culture medium. Black and Finch (1995) evaluated a variety of tissues using a micropartitioning technique for ionizable compounds and found that acrylic acid had tissue:blood partition coefficients that were close to 1:1 for a wide variety of tissues. The similarity of tissue culture medium to blood indicates that equilibrium partitioning of acrylic acid from the medium into cultured epithelial tissues should be close to 1:1. Similarly, the

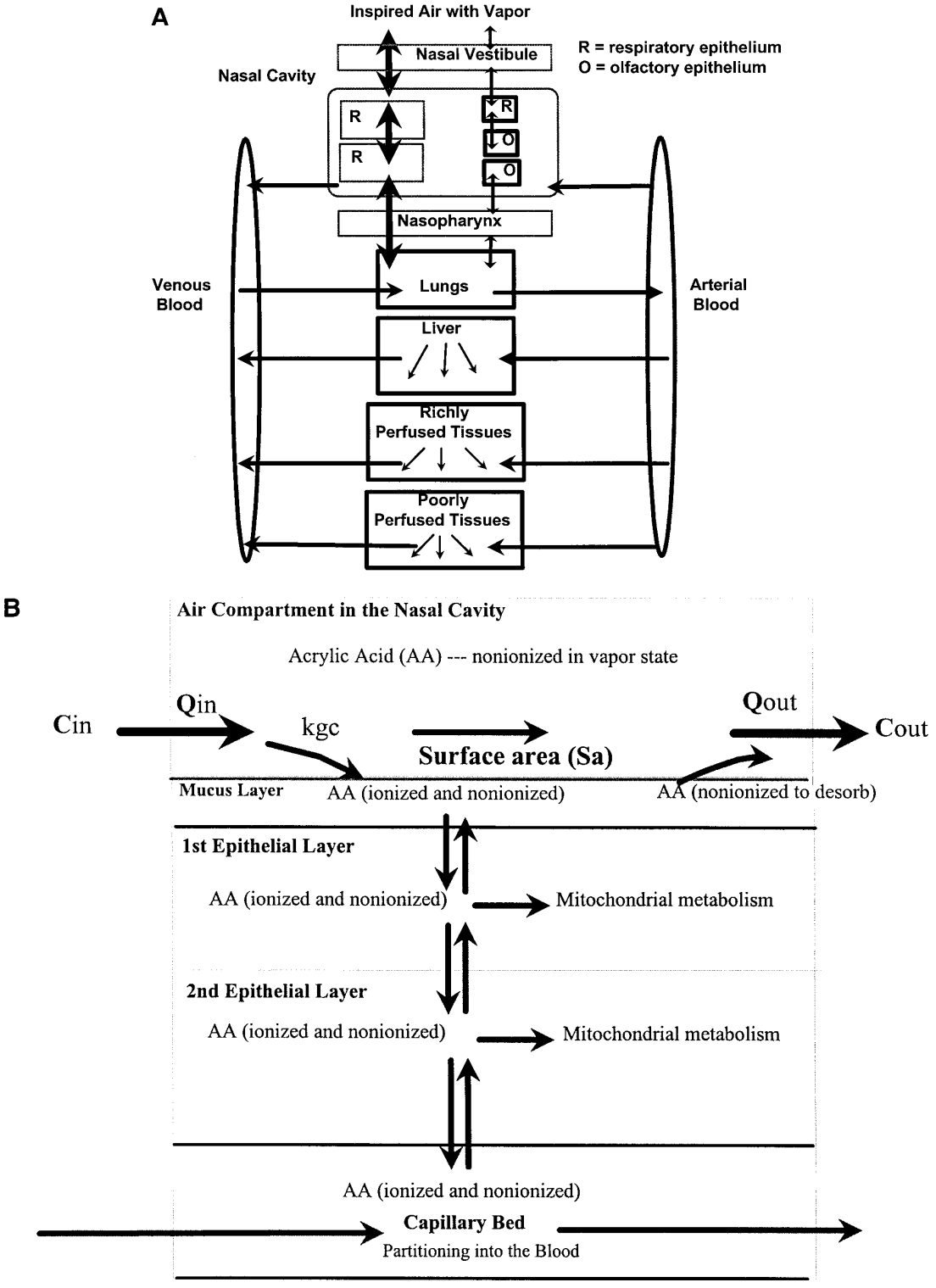

FIG. 2. (A) Diagram of the PBPK model constructed to comprehensively describe the regional nasal deposition, systemic absorption, distribution, and excretion of acrylic acid and (B) to describe the local interaction of inhaled acrylic acid vapors with the nasal epithelium. The rodent model uses two olfactory compartments to incorporate both the olfactory epithelium in the projection extending along the dorsal meatus and the ethmoid olfactory region. The human model uses one olfactory compartment since the human nasal cavity lacks a counterpart for the rodent ethmoid olfactory region. The variable names in the air compartment of B relate to the rate equations of the Appendix.

TABLE 1
Incidence of Histological Lesions in the Nasal Cavity of Rats Exposed to 75 ppm Acrylic Acid Vapor for 3 or 6 h

	0 PPM		75 PPM	
	3 h	6 h	3 h	6 h
Section 1[a]				
Olfactory[b]	0/5	0/5	1/5	1/5
Respiratory[c]	0/5	0/5	0/5	2/5
Section 2				
Olfactory	0/5	0/5	3/5	2/5
Respiratory	0/5	0/5	0/5	0/5
Section 3				
Olfactory	0/5	0/5	2/5	4/5
Respiratory	0/5	0/5	0/5	0/5
Section 4				
Olfactory	0/5	0/5	0/5	4/5
Respiratory	NA[d]	NA	NA	NA

[a] Section number of nasal cavity.
[b] Olfactory epithelial degeneration and sustentacular cell necrosis.
[c] Respiratory epithelial cell degeneration and desquamation.
[d] Not applicable. No respiratory epithelium present.

partitioning between mucus and the underlying tissues is assumed to be close to unity.

Evaluation of Regional Nasal Air Flow and Gas Phase Mass Transport Coefficients from CFD Simulations

CFD simulations conducted with computer models of the rat and human nasal cavities provided estimates of the volume of air flowing through various regions of the rat and human nasal cavities at inhalation flow rates representative of resting to light activity physiological conditions (Tables 4 and 5; anatomical regions are designated in Fig. 1). The data from these CFD simulations confirmed previous studies (e.g. Swift and Proctor, 1977; Hahn *et al.,* 1993; and Keyhani *et al.,* 1995) by indicating that a relatively small fraction of the inspired air ventilates the human olfactory epithelium relative to the rat olfactory epithelium (in this study, approximately 7% in the human relative to approximately 15% in the rat). This difference is greater in the posterior olfactory region of the human nasal cavity (olfactory air flow *decreases* to only approximately 3% of total nasal air flow as the dorsal medial air stream moves ventrally into the medial region) relative to the posterior olfactory region of rats (olfactory air flow *increases* to approximately 20% of total flow as medial air flow contributes to the dorsal medial stream in the posterior region). Other CFD studies have graphically demonstrated this effect with contour maps and "streamlines" of air flow in both the rat nasal cavity (Kimbell *et al.,* 1993) and human nasal cavity (Hahn *et al.,* 1993; Keyhani *et al.,* 1995; Subramaniam *et al.,* 1998).

Generally, where data can be compared, the regional compartmental gas phase mass transport coefficients for the rat nasal cavity are one to two orders of magnitude higher than those of the human nasal cavity (Tables 4 and 5). This indicates that the rat nasal cavity is much more efficient than the human nasal cavity in "scrubbing" an organic vapor from inhaled air (i.e., equilibrating vapor with the nasal mucus layer as opposed to allowing it to reach the downstream tracheobronchial region). Bush *et al.* (1998) noted that the mass transport coefficients calculated for the rat nasal cavity were much higher than would be predicted from simple cylindrical geometry and attributed the difference to the interaction of air flow with the complex geometry of the rat nasal cavity. The observation that the regional mass transport coefficients in the human nasal cavity are closer to those predicted for a cylindrical geometry may reflect less complex air flow patterns and a larger effective lumen volume to mucus surface area ratio than the rat nasal cavity.

The available experimental evidence for the near-quantitative deposition of a variety of highly soluble vapors in the whole rat nasal cavity is supportive of very high mass transport coefficients for the rodent nasal cavity (e.g., 99+% nasal uptake of inhaled hydrogen fluoride vapor; Morris and Smith, 1982). Since the gas phase mass transport coefficients for the rat nasal cavity are so high, the rat nasal dosimetry model of Morris *et al.* (1993), which assumes full equilibration of inhaled vapors with the nasal epithelium (hence, no air phase resistance to nasal deposition), appears to be an accurate ap-

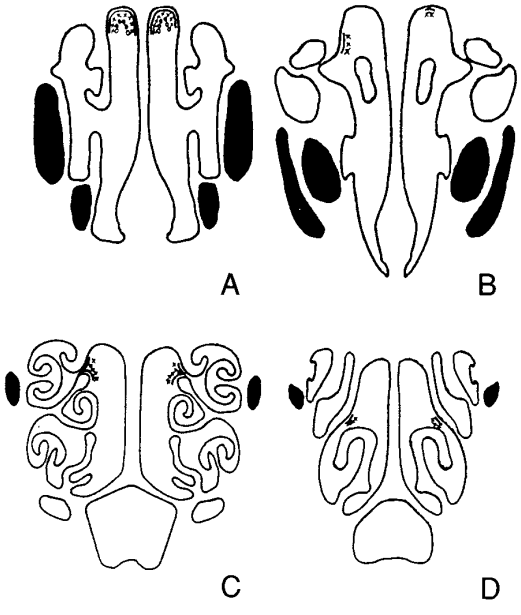

FIG. 3. Composite distribution of nasal lesions of the group of rats exposed once for 6 h to 75 ppm acrylic acid vapor. The templates are taken from Mery *et al.* (1994) and correspond to cross-sections taken at Sections 6 (A), 9 (B), 23 (C), and 26 (D) from Fig. 1 of this reference. The lesions were marked by symbols in the adjacent lumen of the nasal cavity: regions of olfactory epithelial degeneration (solid line), regions of sustentacular cell necrosis (×), and regions of respiratory epithelial degeneration and desquamation (○).

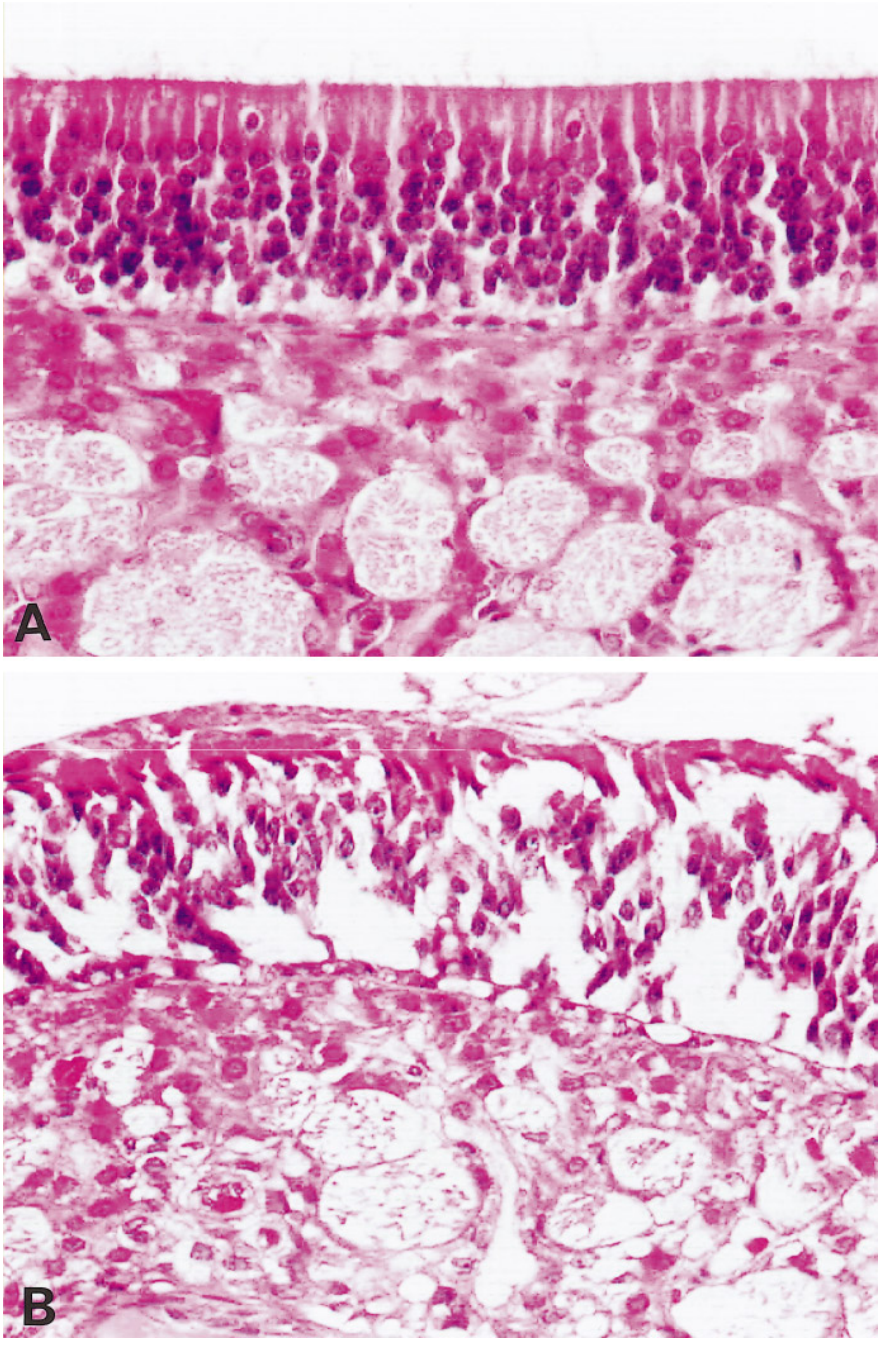

FIG. 4. Olfactory epithelium from a control rat (A) and a rat exposed to 75 ppm AA for 6 h (B). This region of olfactory epithelium from the treated rat demonstrates epithelial degeneration (vacuolation and disassociation) and necrosis of sustentacular cells.

proximation, and rat nasal uptake of vapors may be described as limited by tissue phase resistance (i.e., limited by factors such as diffusion, metabolism, and blood perfusion in the tissue phase). Supporting this conclusion, Bush *et al.* (1998) have used sensitivity analysis in a similar hybrid CFD–PBPK of the nasal deposition of nonmetabolized vapors in the rat nasal cavity to demonstrate that the rate of liquid phase diffusion dominates the extent of uptake in this species.

An important observation noted by Bush *et al.* (1998) for the rat nasal cavity (and replicated in Table 4 of this study) between flow rate and regional mass transport coefficients was also observed in the CFD simulations for the human nasal cavity (Table 5). Generally, the mass transport coefficient *increases* with increasing fluid velocity with simple geometries (flat plate, circular tube, etc.; discussed in Cussler, 1997, Ch. 8). However, in several regions of both the rat and human nasal

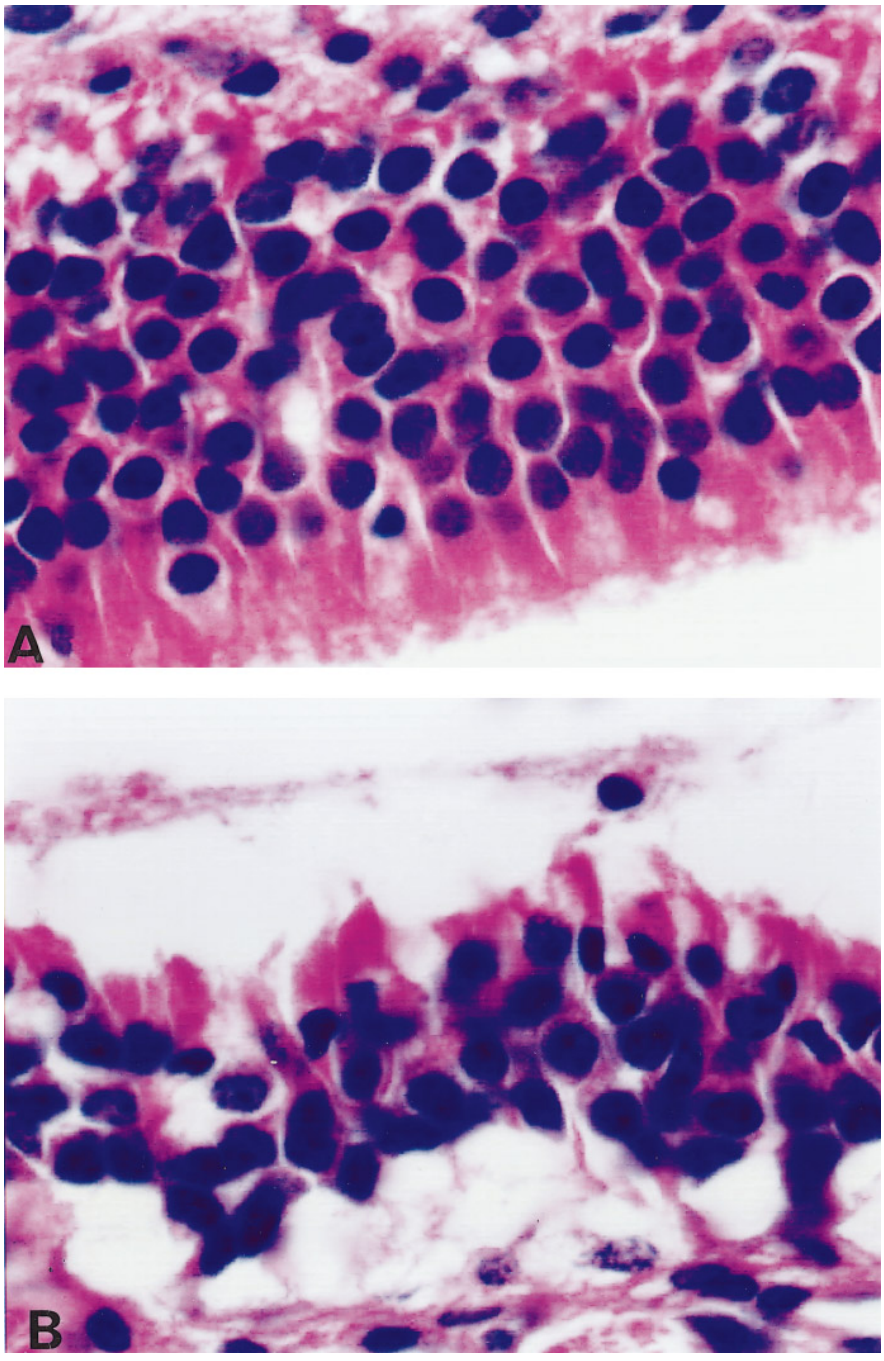

FIG. 5. Olfactory epithelium from the nasal septa of rats incubated either with control tissue culture media (A) or media containing 6 mM AA for 2 h (B). This region of olfactory epithelium from the treated septum demonstrates epithelial degeneration (vacuolation and disassociation) and necrosis of sustentacular cells that is very similar to that observed in the rat nasal cavity from *in vivo* studies (Fig. 4).

cavity (including the olfactory region), the mass transport coefficient *decreases* with increasing flow rate. This anomalous relationship was attributed by Bush *et al.* (1998) to the complex geometry of the air passages in the nasal cavity and the possible detachment of the air boundary layer with increasing flow rate.

Sensitivity analysis of the model parameters in the rat CFD–PBPK model from the base set of values listed in Tables 3 through 6 and the Appendix gave results that were virtually identical to those reported for the 16-compartment model of Bush *et al.* (1998). Notably, the model's predictions of overall nasal uptake were very insensitive to variations in the compartmental gas phase mass transport coefficients (varying the coefficients in Table 4 by a factor of ± 2 produced a change in

TABLE 2
Dose Response for Histopathological Effects in the Epithelium of Rat Nasal Septa Incubated with Acrylic Acid *In Vitro*

Concentration of AA in medium (mM)	Histopathological findings in olfactory epithelium
0	No visible lesions
0.1	No visible lesions
0.2	No visible lesions
0.4	No visible lesions
0.6	Cytoplasmic vacuolation and nuclear swelling of sustentacular cells (2/4)[a]
1.0	Cytoplasmic vacuolation and nuclear swelling of sustentacular cells (4/4)
3.0	Sloughed sustentacular cells (4/4)
6.0	Sloughed sustentacular cells, Sloughed neuroepithelium (4/4)

[a] Number of explants with lesion/number of explants examined.

nasal uptake of less than 1%). However, uptake was sensitive to variation in liquid phase diffusivity (Appendix) and to variation in the mucus:air partition coefficient (Table 3), and the magnitude of this variation was very similar to that reported by Bush *et al.* (1998). In contrast to the rat model, the human CFD–PBPK model was sensitive to variation in air phase parameters in addition to liquid phase parameters. For example, for a CFD–PBPK simulation of acrylic acid vapor uptake at a unidirectional flow rate of 18.9 liter/min, the overall nasal deposition was predicted to be 52% in the human nasal cavity. Varying the air phase mass transport coefficients by factors of -2 and $+2$ from the base case parameters of Table 5 resulted in overall nasal uptake values of 41 and 60%, respectively. Changes in nasal uptake produced by twofold variation in liquid phase diffusivity coefficients (all layers varied simultaneously) and mucus:air partition coefficients were comparable to those changes produced by twofold variations in the gas phase mass transfer coefficients.

The current lack of CFD data for the posterior region of the rat nasal cavity limits interspecies comparisons of the deposition in the *total* nasal cavity somewhat, but the available data for the anterior half of the rat nasal cavity demonstrates that even the anterior half is more efficient in scrubbing organic vapors (approximately 97% at an inspiratory flow rate of 252 ml/min; Kimbell *et al.*, 1993) than the entire human nasal cavity including nasopharynx (approximately 88% at a flow rate of 18,900 ml/min as determined in this study). This comparison is made with "C = 0 boundary conditions" in CFD simulations that only evaluate the contact of the inhaled vapor with the walls of the nasal cavity (i.e., all vapor that contacts the mesh wall is instantly absorbed and no "back pressure" is simulated). On a *regional* basis in the nasal cavity, this interspecies difference in the deposition of inhaled vapors in the overall nasal cavity is significant (see regional nasal dose comparisons below) due to differences in the air flow patterns and distribution of epithelia between the two species. In contrast to the limiting *tissue phase resistance* in the rat nasal cavity, these data clearly indicate that *air phase resistance* to the deposition of inhaled vapors is a significant factor that limits uptake in the human nasal cavity, at least on a regional basis (see Cussler, 1997, for a discussion of the concept of resistances in series relative to mass transfer across a gas–liquid interface; Appendix). In other words, a reasonably accurate nasal dosimetry model for humans must incorporate an air phase compartment to describe the regional air phase rate limitations associated with the deposition of inhaled vapors, rather than assuming full equilibration of inhaled vapors as is appropriate for the rat nasal cavity.

Regional Tissue Dose Estimates from Physiologically Based Inhalation Modeling

A hybrid CFD-PBPK inhalation model (Figs. 1 and 2) was prepared to evaluate the relationship between inhaled acrylic acid vapor concentration (air phase) and the tissue concentration (liquid phase) in various regions of the nasal cavity. The model was designed to easily incorporate interspecies differences in nasal anatomy and air flow patterns via CFD analysis of nasal air flow for each species and to facilitate databased interspecies extrapolation for risk assessment. An explicit effort was made to derive the parameters used in the model either from experimental data or from physicochemical principles (Tables 3 through 6; Appendix) without "fitting" model parameters.

For the rat nasal cavity, the model was used to simulate the air flow distribution from the CFD analysis described by Kimbell *et al.* (1993). However, the distribution of air flow was

TABLE 3
Partition Coefficients of Acrylic Acid between Liquid Phases and Air

Liquid phase (pH)	Liquid:air partition coefficient
Saline (unbuffered)	1450 ± 360[a]
Saline (pH 2.0)	1780
Saline (pH 7.4)	3210
Rat blood (unbuffered)	5500 ± 200
Rat blood (pH 2.0)	6100 ± 350
Rat blood (pH 7.4)	4300 ± 130
Rat fat (unbuffered)	5630 ± 1350
Rat fat (pH 2.0)	2140 ± 710
Rat fat (pH 7.4)	8460 ± 360
Water (unbuffered)	2320
Tissue culture media[b] (pH 7.3)	7800
Octanol	6280
Olive oil	3530

[a] Mean ± SD of triplicate replicates of triplicate analyses. Values listed without a SD are triplicate replicates of a single analysis.

[b] Tissue culture media used for explants of nasal epithelium (see Materials and Methods).

TABLE 4
Results from CFD Simulations of the Deposition of Inhaled Acrylic Acid Vapor in a Model of the Rat Nasal Cavity under "Concentration Equals Zero" Boundary Conditions

Parameter and compartment[a]	Simulation flow rate (ml/min) (100)	(300)	(500)
Regional flow[b] (also regional surface area in cm^2 and lumen volume in cm^3)			
Vestibule (0.44, 0.01)	1.0	1.0	1.0
DM respiratory (0.2, 0.004)	0.12	0.15	0.18
DM olfactory (0.42, 0.012)	0.14	0.15	0.17
Ethmoid olfactory (6.33, 0.054)	0.17	0.19	0.21
Anterior ventral respiratory (1.8, 0.09)	0.88	0.85	0.82
Posterior ventral respiratory (4.5, 0.09)	0.83	0.81	0.79
Nasopharynx (0.1, 0.001)	1.0	1.0	1.0
Regional gas phase mass transport coefficients[c]			
Vestibule (estimated value)	0.004	0.01	0.02
DM respiratory	333.0	134.0	15.3
DM olfactory	134.0	120.0	21.0
Ethmoid olfactory (estimated value)	442.0	1480.0	2710.0
Anterior ventral respiratory	578.0	639.0	1775.0
Posterior ventral respiratory (estimated value)	3083.0	358.0	69.0
Nasopharynx (estimated value)	0.003	0.01	0.017

[a] The regional nasal compartments are defined by epithelial types with the surface areas and lumen volumes for each region derived either from the FIDAP mesh or by difference from Gross *et al.* (1982): Vestibule = anterior region covered with squamous epithelium; DM respiratory = anterior dorsal medial respiratory epithelium; DM olfactory = anterior projection of dorsal medial olfactory epithelium; Ethmoid olfactory = remaining olfactory epithelium covering ethmoid turbinates and septum; Anterior ventral respiratory = anterior region of remaining respiratory epithelium covering the septum and ventral and lateral walls of the nasal cavity; Posterior ventral respiratory = posterior region of remaining respiratory epithelium covering the septum and ventral and lateral walls of the nasal cavity; Nasopharynx = region posterior to the most posterior olfactory epithelium.

[b] Fraction of total air flow entering this region of the nasal cavity (dimensionless).

[c] Gas phase mass transport coefficient (cm/s) calculated from CFD simulations at three flow rates. The simulations were conducted with a gas phase diffusivity of 0.15 cm^2/s and were scaled in the hybrid CFD–PBPK model by a factor of 0.6 for vapor with a gas phase diffusivity of 0.1 cm^2/s. The rat "mesh" used for the CFD simulations replicated the anterior half of the nasal cavity (anterior 16 mm and 18% of the total nasal surface area estimated by Gross *et al.,* 1982), and the simulation did not include uptake in the vestibule, ethmoid turbinate region, posterior ventral respiratory region, and the nasopharynx (Kimbell *et al.*, 1993, 1997). Estimates of K_{gc} for those regions were calculated based on an assumed fractional penetration of 0.999 for the vestibule and nasopharynx (essentially no uptake) and an assumed fractional penetration of 1.0×10^{-4} for the ethmoid olfactory region and the posterior ventral respiratory region (based on representative values from modeling of the anterior compartments).

divided into two air flow streams similar to the approach used by Morris *et al.* (1993): a dorsal medial that corresponded to the dorsal medial flow stream described by Kimbell *et al.* (1993), and the remaining four ventral and lateral streams described by Kimbell *et al.* (1993) were combined into one flow stream (Figs. 1 and 2A). This approach was simpler than the more sophisticated air flow analysis of the rat nasal cavity conducted by Bush *et al.* (1998), because the available human data for interspecies tissue dose comparisons were limited. As noted in Materials and Methods, the rat olfactory epithelium was divided into an anterior dorsal meatus projection (7% of the surface area of the nasal cavity) and a much larger posterior ethmoid region (44% of the surface area of the nasal cavity). In the *in vivo* inhalation studies that have been conducted, inhalation of an irritating organic acid or ester has resulted in an anterior-to-posterior progression of lesions that parallels the dose–response curve (i.e., the most anterior dorsal–medial olfactory epithelium exhibits the lesions observed at the lowest inhaled concentrations that induce a toxic effect). Consequently, for interspecies extrapolation, comparisons of tissue concentrations were based on the first epithelial layer of this anterior compartment of olfactory epithelium lining the dorsal meatus region of the rat nasal cavity. This is the olfactory region that is exposed to the highest vapor concentration and would be the first region to demonstrate toxicity in a dose–response study. As noted above, this region also contains the apical cell bodies of the acid-sensitive sustentacular cells of the olfactory epithelium. Since the human nasal cavity only has a small area covered with olfactory epithelium (approximately 4% of the surface area of the nasal cavity; Lang, 1989) and no anatomical equivalent for the ethmoid turbinates, this region was described by one compartment, but with the same number of cell layers as in the rat.

The output of the rat CFD–PBPK model was evaluated by comparing the predicted fractional nasal uptake for acrylic acid with the data from a unidirectional uptake study (Morris and Frederick, 1995. The predicted uptake from the model for unidirectional flow, 98%, compares favorably with the mea-

TABLE 5
Results from CFD Simulations of the Deposition of Inhaled Acrylic Acid Vapor in a Model of the Human Nasal Cavity under "Concentration Equals Zero" Boundary Conditions

Parameter and compartment[a]	Simulation flow rate (ml/min)		
	11,400[b]	18,900[b]	18,900[c]
Regional flow[d] (also regional surface area in cm^2 and lumen volume in cm^3)			
Vestibule (32.4, 4.83)	1.0	1.0	1.0
DM respiratory (10.1, 0.74) entering region =	0.079	0.084	0.084
DM olfactory (13.2, 0.56) entering region =	0.060	0.069	0.069
DM olfactory (13.2, 0.56) exiting region =	0.025	0.027	0.027
Ethmoid olfactory	NA[e]	NA	NA
Anterior ventral respiratory (42.1, 3.50)	0.921	0.916	0.916
Posterior ventral respiratory (72.3, 5.16)	0.940	0.931	0.931
Nasopharynx (75.8, 18.32)	1.0	1.0	1.0
Regional gas phase mass transport coefficients[f]			
Vestibule	2.33	3.28	2.31
DM respiratory	6.44	5.0	3.23
DM olfactory	117.0	32.9	22.8
Ethmoid olfactory	NA	NA	NA
Anterior ventral respiratory	3.78	6.25	2.64
Posterior ventral respiratory	5.19	5.14	3.24
Nasopharynx	2.14	2.61	1.59

[a] The regional nasal compartments are defined by epithelial types as described in Table 5. The surface areas and lumen volumes for each region are derived from the FIDAP mesh. The human nasal cavity does not have an ethmoid olfactory region, consequently the human nasal computer model does not have this compartment.

[b] Simulation conducted with a gas phase diffusivity of 0.15 cm^2/s.

[c] Simulation conducted with a gas phase diffusivity of 0.1 cm^2/s.

[d] Fraction of total air flow entering each region of the nasal cavity (dimensionless). In the olfactory region, there was a significant loss of air flow between the anterior and posterior faces of the region. This loss of air flow is accounted for in the posterior ventral respiratory region of the model.

[e] NA, not applicable to this species.

[f] Gas phase mass transport coefficient (cm/s).

sured value, 97 ± 1%. To further assess the capabilities of the model, the rates of ionization and metabolism were set to zero and the appropriate mucus:air partition coefficients were substituted to simulate the flow-dependent unidirectional uptake of a wide variety of relatively poorly metabolized vapors (partition coefficients and uptake data from Morris *et al.*, 1993). For this exercise, the air phase and liquid phase diffusion coefficients were not varied from the CFD/PBPK model's base set of parameters (Table 4; Appendix I). The CFD–PBPK model replicated the overall fractional nasal uptake of these vapors very well (Fig. 6) with performance very similar to the related 16-compartment rat model for nonmetabolized vapors on which this model was based (Bush *et al.*, 1998).

In addition, unidirectional simulations were conducted with the acid model at a flow rate of 500 ml/min to estimate the steady-state tissue concentration in the anterior olfactory epithelium lining the dorsal meatus of the rat nasal cavity over a wide range of acrylic acid vapor concentrations (Fig. 7). From simulations conducted at an inhaled acrylic acid concentration of 75 ppm, the predictions of the CFD-PBPK model for the concentration of acid in the dorsal medial olfactory epithelium were compared to the dose–response data from the *in vitro* nasal explant study with acrylic acid. The model prediction of 10.7 mM acrylic acid concentration in the sustentacular cell layer of the olfactory epithelium in the dorsal meatus was correlated with the olfactory histopathology observed *in vivo* (Table 1; Fig. 4). The *in vivo* histopathology is reasonably consistent with the cytotoxicity observed in the *in vitro* nasal explant studies at 6 mM (Table 2; Fig. 5), which is within a factor of approximately two of the model prediction. Repeating the simulated exposure of a rat to 75 ppm acrylic acid under representative cyclic breathing conditions (ventilation as described in Fig. 8) resulted in a somewhat lower predicted olfactory tissue concentration, 5.2 mM, which correlated more closely with the explant histopathology data.

Although cytotoxicity was observed in the rat ethmoid olfactory region following the 75 ppm exposure, it was much less severe and extensive than that observed in the dorsal meatus region. The unidirectional flow tissue dose prediction of the model (3.0 mM in the ethmoid olfactory region) is consistent with this observation given the transition in histopathology observed in the 1 to 3 mM dose range *in vitro* (Table 2). Although there is inherent variability in comparing histopathology observed *in vitro* to that observed *in vivo* (based on medium effects, differences in oxygenation, the highly localized pattern of the lesions observed *in vivo*, etc.), the acute

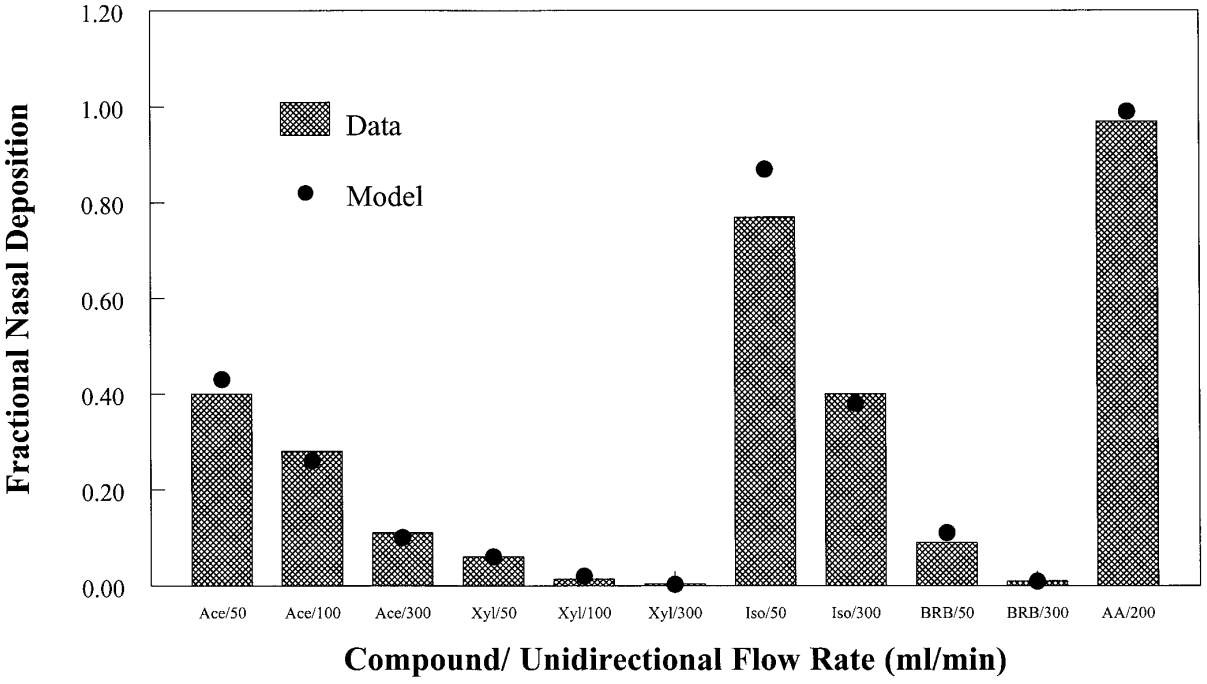

FIG. 6. Comparison of CFD–PBPK model predictions to the unidirectional rat nasal deposition data of Morris *et al.* (1993) for a variety of vapors at differing flow rates. The filled circles represent the predictions of the model based on the liquid:air partition coefficient of each vapor (Morris *et al.*, 1993) and the listed air flow rate in ml/min. The liquid phase diffusion coefficients were not varied from the model base set of parameters (Appendix and Table 4), except that the vapor metabolism and ionization rates were set to zero. ace, acetone; xyl, xylene; iso, isoamyl alcohol; BRB, bromobenzene; AA, acrylic acid.

cytotoxic response of the sustentacular cells in both environments suggests that this tissue–dose comparison may be useful as a rough approximation for evaluating the predictions of the CFD–PBPK model. Given the "lumping" that is inherent in constructing a compartmental dosimetry model and the fact

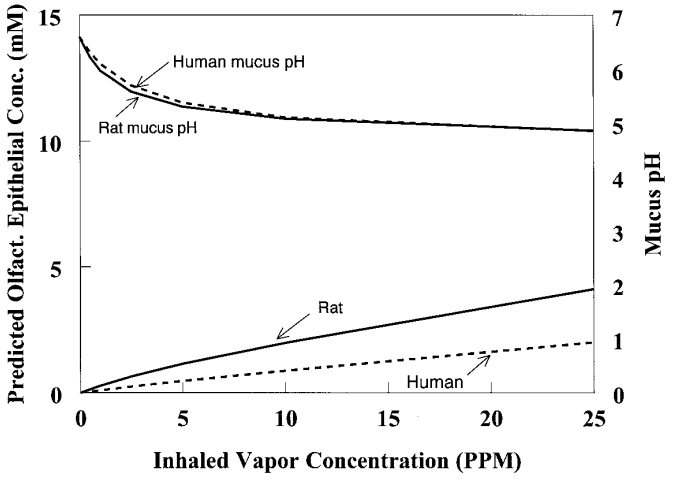

FIG. 7. The predicted relationships from the CFD–PBPK model between the concentration of inhaled acrylic acid vapor and the tissue concentration of acrylic acid and mucus pH in the most anterior dorsal region of the olfactory tissue in the nasal cavity of the rat (solid lines) and humans (dashed lines) under comparable steady-state unidirectional flow (twice the resting minute volume for a 1-h simulation) for each species.

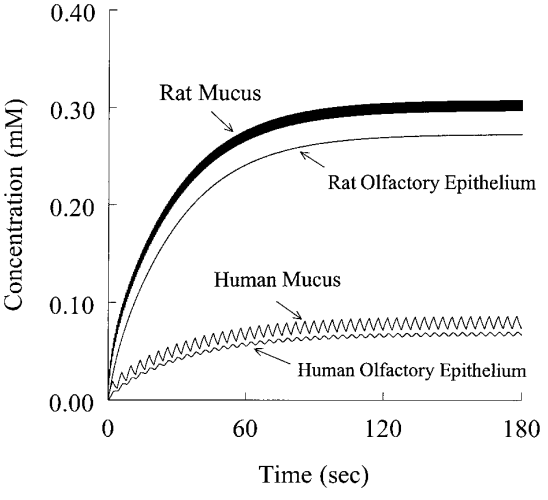

FIG. 8. Predicted concentrations from CFD–PBPK model simulations of absorbed acrylic acid vapor in the olfactory region of a rat and human under simulated breathing conditions. The cyclic flow simulation was conducted for a reference resting rat and human exposed to 2 ppm acrylic acid for 3 min. The respiration of an adult rat was simulated at a representative respiration rate of 150 breaths/min (too fast to resolve individual breaths in this figure) and a tidal volume of 1.7 ml/breath to give a minute volume of 250 ml/min (EPA, 1994). Similarly, an adult human was simulated with a respiration rate of 15 breaths/min and a tidal volume of 500 ml/breath (ICRP, 1975). The predicted concentrations were for the mucus layer overlying the olfactory epithelium and the apical anterior layer of olfactory epithelium, which primarily consists of acid-sensitive sustentacular cells.

that the model simulation did not include exposure-related changes in breathing rate or physiology, it is not surprising that the unidirectional flow model predictions did not exactly correspond to the histopathology observed with the nasal epithelial explants *in vitro*. Notably, the model predictions in the above comparisons were made without "fitting" parameters to the datasets.

The dose–response curve for acrylic acid in olfactory tissue in the rat nasal cavity that was used for the nasal explant tissue dose comparison (Fig. 7) was also used for an interspecies tissue dose comparison. For this exercise, a dose response of acrylic acid exposures was simulated for an adult resting male rat and an adult resting male human using the appropriate inspiratory flow rate (based on the minute volumes of each species), nasal anatomy, and nasal air flow patterns from CFD simulations. The resulting dose–response relationships of olfactory tissue concentration relative to inhaled vapor concentration for each species were then compared (Fig. 7). In addition, the change in mucus pH over the olfactory epithelium was estimated as the buffer in the mucus was depleted to neutralize the deposited acidic vapor. The output from these simulations indicates that the olfactory epithelium in the dorsal meatus region of the rat nasal cavity is exposed to two- to threefold greater concentrations of acid vapor than the human olfactory epithelium under either unidirectional flow (Fig. 7) or cyclic flow (Fig. 8) conditions. The magnitude of this difference changes somewhat based on the inhaled vapor concentration (e.g., threefold or greater at vapor concentrations less than 0.5 ppm, and threefold decreasing to twofold over the 0.5 to 25 ppm vapor concentration range for unidirectional flow; Fig. 7) and differences in the relative size and respiratory physiology of the individuals that are simulated, but generally the olfactory epithelium of humans is predicted to be exposed to significantly lower concentrations of inhaled acids than rat olfactory epithelium. Additionally, the predicted pH of the mucus covering the rat olfactory epithelium fell to slightly lower concentrations than the predicted human mucus pH at occupationally relevant exposure concentrations (less than 10 ppm). The drop in mucus pH could be a factor contributing to the cytotoxicity observed in the apical sustentacular cells, which lie immediately under the mucus layer. Typically, the sustentacular cells have been reported to be the cells that are most sensitive to acidic vapors (e.g., Miller *et al.*, 1981).

To conduct an interspecies nasal tissue dose comparison under a realistic cyclic breathing exposure scenario, a simulated exposure was conducted at the American Conference of Governmental Hygienists (ACGIH) TLV value for acrylic acid of 2 ppm using the same base set of physiological parameters (Table 6). As described in Fig. 8, the rodent tissue concentrations tend to be significantly higher than human tissue concentrations. An exception is the ventral posterior region of the human nasal cavity that is lined with respiratory epithelium. Comparison of the tissue dose values with the histopathology observed in the *in vitro* nasal explant experiments (Table 2) suggests that no toxicity would be predicted in the sensitive human olfactory tissue at this exposure concentration (supportive of the ACGIH recommendation). The highest tissue concentrations (0.66 mM) are predicted to occur in the respiratory epithelium lining the anterior region of the dorsal meatus (respiratory "patch" in Fig. 1), however, no toxicity was observed in respiratory epithelium in the explant studies with acrylic acid concentrations as high as 6 mM.

DISCUSSION

These experiments describe the acute effects of a representative organic acid on the rodent nasal cavity. Interspecies extrapolation of these results to humans was then conducted using a hybrid CFD–PBPK computer model of the rat and human nasal cavity. The histopathological results of this acute study are consistent with the histopathological observations from subchronic and chronic inhalation studies on a wide variety of organic acids and esters (e.g., Keenan *et al.*, 1990; Trela and Bogdanffy, 1991; Miller *et al.*, 1981, 1985; Reininghaus *et al.*, 1991). Olfactory epithelium in the anterior region of the nasal cavity is preferentially targeted, although respiratory epithelium is affected at high acid or ester concentrations or with particularly strong acids. In the rat, a narrow strip of olfactory epithelium protrudes anteriorly along the dorsal surface of the nasal cavity in the region described as the dorsal meatus. Immediately anterior to the sensitive olfactory epithelium is a very small patch of respiratory tissue that is only a few millimeters wide. This dorsal meatus region receives 12 to 21% of the inhaled air (Kimbell *et al.*, 1993 and this study), and rodent inhalation studies with acids and esters typically result in histopathological damage to this poorly protected olfactory epithelium. Increasing concentrations and longer durations of vapor exposure typically result in a broader posterior distribution of olfactory lesions into the ethmoid turbinates in the posterior region of the nasal cavity. The tissue dose distribution associated with this histopathological observation is reproduced in the current inhalation model. At high concentrations of inhaled vapor, the mucus layer in the anterior part of the nose becomes saturated with vapor. This decreases the driving force for deposition in the anterior portion of the nose, thereby allowing more vapor to reach the posterior regions of the nasal cavity. In this context, a "high" vapor concentration is dependent on the combination of gas phase and liquid phase characteristics of the vapor that result in a significant accumulation of the vapor in the mucus, which can inhibit further deposition of the vapor.

The use of histopathology from short-term organ culture studies to estimate tissue concentration *in vivo* is only possible with compounds that induce readily observable cytotoxicity relatively quickly. In this case, the sensitive sustentacular cells provide support for the olfactory neurons, and the histological changes in the structure of the epithelium that are associated with cytotoxicity are rapidly apparent. Although these *in vitro*

TABLE 6
Anatomical, Physiological, and Metabolic Parameters for the Rat and Human Nasal PBPK Models

Parameter	Value	Source
Rat (adult male F344 under chronic exposure conditions)		
Minute volume[a] (ml/min)	250	(EPA, 1994)
Body weight (g)	380	(EPA, 1994)
Lung volume[b]	0.004	(Delp *et al.*, 1991)
Liver volume	0.035	(Delp *et al.*, 1991)
Muscle and fat volume	0.40	(Delp *et al.*, 1991)
Other tissues	0.41	(Delp *et al.*, 1991)
Venous blood volume	0.06	(Delp *et al.*, 1991)
Arterial blood volume	0.03	(Delp *et al.*, 1991)
Blood flow to liver[c]	0.173	(Delp *et al.*, 1991)
Blood flow to muscle and fat	0.35	(Delp *et al.*, 1991)
Blood flow to other perfused tissues	0.466	(Delp *et al.*, 1991)
Blood flow to nasal cavity	0.01	(Stott *et al.*, 1986)
Blood flow to nasopharynx	0.001	Estimate
Human (adult male under chronic exposure conditions)		
Minute volume (ml/min)	7500	(ICRP, 1975)
Body weight (g)	70000	(ICRP, 1975)
Lung volume	0.014	(ICRP, 1975)
Liver volume	0.026	(ICRP, 1975)
Muscle and fat volume	0.60	(ICRP, 1975)
Other tissues	0.20	(ICRP, 1975)
Venous blood volume	0.046	(ICRP, 1975)
Arterial blood volume	0.014	(ICRP, 1975)
Blood flow to liver	0.25	(Williams and Leggett, 1989)
Blood flow to muscle and fat	0.22	(Williams and Leggett, 1989)
Blood flow to other perfused tissues	0.519	(Williams and Leggett, 1989)
Blood flow to nasal cavity	0.01	Estimate
Blood flow to nasopharynx	0.001	Estimate

[a] Unidirectional flow simulations with the nasal dosimetry model were conducted at twice the minute volume as an approximation of the plateau peak inspiratory flow rate. Minute volumes for each species are for resting ventilation.
[b] Tissue volumes are expressed as a fraction of body weight.
[c] Blood flow is expressed as a fraction of cardiac output. Cardiac output is 14,000 ml/h allometrically scaled to body weight in kg to the 0.74 power.

and *in vivo* histopathology comparisons may be useful for semiquantitative tissue dose estimates, there are intrinsic differences in the response of tissues cultured *in vitro* relative to those exposed *in vivo* that may limit the accuracy of this method.

The histological structure of olfactory epithelium varies little between mammalian species (e.g., Nakashima *et al.*, 1984, 1991; Uraih and Maronpot, 1990; Talamo *et al.*, 1995). Furthermore, the mode of action for cytotoxicity of inhaled short chain organic acid vapors, mitochondrial toxicity, is assumed to be fundamentally the same across species (e.g., Sherrat, 1985; Brass, 1994; Custodio *et al.*, 1998). These factors suggest that the susceptibility of the tissue to inhaled irritants also varies relatively little between mammalian species. If this is the case, the dominant factor influencing interspecies differences in susceptibility to inhaled irritants is olfactory tissue dose. However, the potency of inhaled irritants as olfactory cytotoxicants clearly varies. Strong acids (e.g., formic acid) damage respiratory and olfactory epithelium whereas weaker acids (e.g., acrylic acid) primarily damage the olfactory epithelium. Risk assessments for these vapors may incorporate an estimate of potency from the NOAEL of a rodent inhalation study and model-derived interspecies tissue dose comparisons (using the appropriate compound-specific parameters) to assist in establishing appropriate human exposure limits.

The available data linking a dosimeter with the cytotoxicity induced by short chain organic acids such as acrylic acid suggests that tissue concentration of the acid (in its primarily ionized form) is the most appropriate dose measure for interspecies extrapolation and risk assessment. Notably, the nasal epithelial explant studies in this study were conducted with the neutralized acid in the tissue culture medium, which equilibrated with the explants with a partition coefficient of approximately one. The most direct interpretation of this data is that the observed olfactory cytotoxicity was correlated with the concentration of the neutralized acid in the medium and by implication in the tissue. Similarly, the recent studies indicating that neutralized acrylic acid induces the glutathione-independent mitochondrial permeability transition with isolated rat liver mitochondria *in vitro* (Custodio *et al.*, 1998) suggest that

the steady-state concentration of the neutralized acid in the mitochondrial environment is the appropriate dosimeter.

An explicit advantage of the CFD–PBPK dosimetry model is that it facilitates description of the dynamic relationship between tissue concentration and metabolism (and/or tissue reactivity) with the concentration of the vapor in the air stream. Cyclic air flow (inhalation and exhalation) can also be modeled (e.g., Fig. 8) to evaluate factors such as desorption from mucus during exhalation (Gerde and Dahl, 1991) and to provide an estimate of net uptake under simulated breathing conditions. Comparison of cyclic flow modeling exercises to unidirectional flow exercises at the same concentration of acrylic acid vapor suggest a lower steady-state concentration of the vapor in the nasal epithelium under cyclic flow conditions. This is presumably due to the partial clearing of the vapor from the epithelium by diffusion into the blood and by desorption during exhalation. Inclusion of a "body" in the CFD–PBPK model (e.g., a description of systemic circulation, distribution to peripheral compartments, and metabolism) provides dynamically changing boundary conditions for the nasal cavity during simulations as the arterial blood concentration changes as a function of exposure time.

A technical aspect of the description of mass transport of the vapor at the air:mucus interface in the CFD–PBPK model bears some elaboration. As described more fully in the Appendix, the term "mass transport coefficient" has multiple definitions depending on the context in which it is used. A unique aspect of the CFD–PBPK model used for this study is the definition of a "compartmental mass transport coefficient" (Appendix). The definition and use of this value is consistent with principles described in a recent text on this subject (Cussler, 1997), and this term has distinct theoretical and practical advantages for linking CFD data with compartmental PBPK models. Specifically, it facilitates the translation of CFD data into a form commonly used in pharmacokinetics (a compartmental clearance value), and it allows the straightforward use of well-mixed compartment descriptions for both the air phase and liquid phase compartments. An alternative definition for the mass transport coefficient (a "distributed mass transport coefficient" based on local concentration differences linked to local mass transport coefficients) is commonly associated with CFD simulations, but its direct use in a compartmental PBPK model is problematic based on theoretical and practical differences in the definition and use of an "average concentration" in the air phase of a CFD study relative to the well-mixed compartmental assumptions that are commonly used for the liquid phase of PBPK models. This inconsistency is not readily apparent in various formulations of rodent CFD–PBPK models. This is because the most readily available experimental data, fractional deposition of inhaled vapors in the overall the rat nasal cavity, are relatively insensitive to significant variation in the rodent gas phase mass transport coefficients (Bush *et al.*, 1998). In fact, as an approximation, Bush *et al.* (1998) were able to successfully use distributed mass transfer coefficients with concentrations calculated for well-mixed air compartments to describe whole-nose deposition of a variety of vapors in the rat nasal cavity. However, the calculated deposition of inhaled vapors in the human nasal cavity is much more sensitive than the rat to variation in the value of the gas phase mass transport coefficients. Therefore, a more accurate mathematical description of the compartmental vapor phase concentration gradient with the accompanying assumptions used for the definition and calculation of the corresponding mass transport coefficient was required. An expedient test of the accuracy of the concentration/mass transport coefficient descriptions is the replication of the CFD simulation uptake results (whole nose) with the hybrid CFD–PBPK model. To do this, a very fast rate of vapor decomposition in the mucus and/or a very high mucus:air partition coefficient may be defined in the CFD–PBPK model to simulate the "C = 0" boundary conditions used in the CFD simulations. Under these conditions, the hybrid CFD–PBPK described in this study exactly replicated the CFD simulation results. Therefore, the use of compartmental mass transport coefficients and well-mixed air compartments in the CFD–PBPK model appears to be sufficiently accurate in both species to be useful for interspecies extrapolation.

Satisfactory performance of the model relative to relevant experimental data, as well as design criteria that we have previously listed (Frederick *et al.*, 1994), suggests that the CFD–PBPK model structure is robust relative to a variety of biological endpoints. In addition, satisfactory performance in the prediction of whole nose uptake of a wide range of poorly metabolized vapors suggests that the basic model structure may have wide applicability. Furthermore, coupling of the nasal dosimetry model with a compartmental PBPK model of the body allows facile dosimetry for all three classes of inhaled vapors that are currently described in the RfC guidelines of the EPA (Environmental Protection Agency, 1994). The CFD–PBPK model may be extended to include a more extensive description of the conducting airways, to model other species by incorporating additional CFD analyses, and to incorporate interindividual variability in nasal anatomy and air flow patterns.

In summary, a useful CFD–PBPK inhalation model has been prepared for interspecies extrapolation of tissue dose in the olfactory region of the nasal cavity. The model output is consistent with whole-nose fractional deposition data for acrylic acid and a wide range of poorly metabolized vapors in rodents. In addition, the model predicts olfactory tissue concentrations for acrylic acid that correlate with acute histopathological lesions observed *in vivo* and with those observed *in vitro* with nasal explants. The model was used to evaluate an acrylic acid vapor exposure concentration that is used as an occupational exposure limit, and the results of the exercise were supportive of the professional judgment used to establish the exposure limit. Generally, the model predicts that under similar exposure conditions (e.g., equal external vapor concen-

tration and equivalent physical activity conditions) human olfactory epithelium is exposed to lower concentrations of inhaled organic acid vapors than rodent olfactory epithelium.

APPENDIX

The general CFD–PBPK model structure is based upon an elaboration of a nasal model proposed by Morris *et al.* (1993) to include systemic compartments with a description of perfusion in each tissue (Frederick *et al.*, 1992, 1994). However, the most unique aspect of the current model is its dynamic description of vapor equilibration at the air:mucus interface as described in more detail in a companion manuscript on the nasal deposition of poorly metabolized vapors (Bush *et al.*, 1998). Notably, the hybrid CFD–PBPK model incorporates a unique compartmental description of both the air phases and underlying tissue phases in the nasal cavity as well as the data from CFD simulations of air flow in the nasal cavity of rats and humans (Kimbell *et al.*, 1993, 1997; Subramaniam, 1998). Although the tissue phase of the model may be easily tailored to describe the nasal deposition of a wide variety of inhaled vapors as described in Fig. 6 (e.g., by incorporating each vapor's unique tissue:air and tissue:blood partition coefficients, tissue-phase metabolism, diffusivity, and reactivity), the primary focus of this study is the development of a model tailored to simulate the ionization and metabolism of inhaled organic acids.

Description of Gas Phase Mass Transport

Although descriptions of mass transport of vapors across an air:liquid interface date back over 70 years, the description of mass transport of an inhaled vapor across the air:mucus interface used for this study relies heavily upon the methods of estimation described by Lyman *et al.* (1990). The general theory associated with interfacial mass transport has been extensively discussed and applied by Cussler (1997). This approach follows the two-film concept for estimating the flux of volatiles across an air:liquid interface.

$$N = K_g\,(C_g - C_l/P)\ , \qquad (1)$$

where

N = flux (μmol/[cm^2 $\times$ h])
K_g = overall mass transfer coefficient (cm/h)
C_g = concentration in gas phase (μmol/cm^3)
P = the liquid:air partition coefficient (dimensionless) and
C_l = concentration in liquid phase (μmol/cm^3).

Cussler (1997) notes that this commonly used equation is basically derived from empirical arguments like those used to derive Fick's law and that the equation conceals a variety of approximations and ambiguities. The most critical problem contributing to this ambiguity is the lack of adequate definitions for the concentrations that determine the concentration gradient. Is it a "local mass transport coefficient" based on "local concentration" differences, or is it an "average mass transport coefficient" based on a difference in "average concentrations" in two compartments or phases? If "average concentrations" are used, how is the "average" defined for each phase? These questions are addressed below for the specific case of the CFD–PBPK model, but it is important to note that a different approach may be more appropriate in other contexts.

The overall mass transport coefficient from the air phase, K_g, into the liquid phase in Equation 1 may be further defined by:

$$1/K_g = 1/k_g + 1/(Pk_l)\ , \qquad (2)$$

where

k_g = gas phase mass transfer coefficient (cm/s) and
k_l = liquid phase mass transfer coefficient (cm/s).

Cussler (1997) notes that the gas phase mass transfer coefficient (k_g, a component of K_g in Equation 2 above) has multiple definitions with correspondingly different units, and he lists four different commonly used definitions. Clearly, the use of the term "mass transport coefficient" without adequate contextual definition contributes to confusion. The following text will derive and define the "compartmental mass transport coefficient" used in this study (i.e., an "average mass transfer coefficient" based on a difference in "average compartmental concentrations"). The use of this form of mass transport coefficient was required by the common use of "well-mixed compartments" in the compartmental modeling of PBPK models, and the need to appropriately express the results of the CFD simulations so that the "average air compartment concentration" derived from the CFD exercise would be defined in the same way as the "average tissue compartment concentration" in the PBPK model. If these "average concentrations" are not commonly defined, an error of variable magnitude that is dependent on airway geometry and the extent of fractional uptake of the vapor will be introduced into the CFD–PBPK model.

By multiplying both sides of Equation 1 by the surface area of the air:liquid interface for a defined compartment, the net mass transport across the interface can be expressed as

$$QS_cN = S_cK_g(C_g - C_l/P)\ , \qquad (3)$$

where

Q_v = net rate of mass transport across an air:liquid interface (μmol/h) and

S_c = surface area of the compartmental air:liquid interface (cm^2).

The air phase mass transport coefficient, k_g, can be estimated by CFD simulations at several representative inhalation flow rates for the differing nasal lumen geometries of various species using defined boundary conditions for the nasal cavity (e.g., by defining a very large value for P to effectively establish a "$C_l = 0$" boundary condition for the simulation such that $k_g \approx K_g$ in Equation 2).

For gas phase compartments in the nasal cavity (Fig. 2B), a compartmental k_g, designated k_{gc}, can be calculated from the CFD simulation results by the following method. Assuming that the compartment is well mixed (i.e., the concentration of the vapor in the gas phase that exits the compartment is the uniform equilibrated concentration in the compartment, i.e., $C_g = C_{out}$), the steady-state mass balance for vapor phase deposition in a compartment in the nasal cavity may be expressed as

$$\sum C_{in}Q_{in} = \sum C_{out}Q_{out} + S_cK_{gc}\,(C_{out} - C_l/P)\,, \qquad (4)$$

where

Q_{in} = flow rate of air entering the nasal compartment (cm^3/h)
Q_{out} = flow rate of air exiting the nasal compartment (cm^3/h)
C_{in} = concentration of vapor in the air entering the nasal compartment ($\mu mol/cm^3$)
C_{out} = concentration of vapor in air exiting the nasal compartment ($\mu mol/cm^3$); this concentration is assumed to be well equilibrated with the steady-state processes of the nasal cavity (including nasal epithelial uptake) and is assumed to be the uniform concentration in the compartment based on the well-mixed compartment model
C_l = concentration in liquid phase ($\mu mol/cm^3$)
S_c = epithelial surface area of the nasal compartment (cm^2) and
K_{gc} = compartmental mass transfer coefficient (cm/h).

By conducting CFD simulations with a "$C_l = 0$" boundary condition for the compartment (effectively assuming that P is very large and therefore $K_{gc} \cong k_{gc}$ according to the relationship that defines K_g) and assuming negligible change in air flow across the compartment (i.e., $Q_{in} = Q_{out} = Q$), the equation simplifies to

$$C_{in}Q = C_{out}Q + S_cK_{gc}C_{out} = C_{out}Q + S_ck_{gc}C_{out} \qquad (5)$$

This allows calculation of a compartmental k_{gc} from the data for the compartmental clearance of the vapor from the gas phase by recognizing that $C_g = C_{out}$ for a well-mixed compartment;

$$C_{out}/C_{in} = \frac{Q}{Q + (S_ck_{gc})}\,, \qquad (6)$$

where C_{out}/C_{in} = the fractional penetration (F_{pet}) or the dimensionless fraction of the vapor that penetrates through a nasal compartment and enters the next compartment. Note that if either k_{gc} or S_c is very large, the denominator becomes large, and the right-hand side of the equation approaches zero fractional penetration.

Solving for k_{gc} after substituting F_{pet} for C_{out}/C_{in} results in:

$$k_{gc} = \frac{Q(1 - F_{pet})}{F_{pet}S_c}\,. \qquad (7)$$

Data from CFD simulations at various flow rates for each species can be used to calculate k_{gc}, since the regional Q, S_c, and F_{pet} can be evaluated for any defined compartment of the nasal mesh as long as a "$C_l = 0$" boundary condition is used.

Although this derivation utilizes common mass transport and fluid dynamics terminology, the underlying theory is very similar to common pharmacokinetic principles that use the hepatic extraction ratio to calculate hepatic clearance (e.g., Gibaldi, 1991; Shargel and Yu, 1993), and K_{gc} may be considered to be analogous to a tissue clearance term used in compartmental pharmacokinetic studies.

An overall mass transfer coefficient from the gas phase, K_{gc}, can now be estimated that combines a compartmental mucus phase mass transport coefficient k_{mc} (analogous to the liquid phase mass transport coefficient k_l in the definition of K_g) with the gas phase mass transport coefficient k_{gc} that was calculated above from CFD simulations that used a $C = 0$ boundary condition (c.f. Hanna *et al.*, 1989; Lyman *et al.*, 1990; Cussler, 1997) as follows:

$$1/K_{gc} = 1/k_{gc} + 1/(Pk_{mc})\,, \qquad (8)$$

where

K_{gc} = overall compartmental mass transport coefficient from the air phase (cm/s)
k_{gc} = compartmental gas phase mass transfer coefficient (cm/s)
k_{mc} = compartmental mucus phase mass transfer coefficient (cm/s) and
P = the liquid:air partition coefficient (dimensionless).

The mucus phase mass transport coefficient, k_{mc}, was formulated as described by Bush *et al.* (1998) to describe transport to the midpoint of the mucus layer:

$$k_{mc} = D_{muc}/(l_{muc}/2)\,, \qquad (9)$$

where

D_{muc} = diffusivity of the compound (primarily the ionized acid) in the mucus phase (cm^2/h) and
l_{muc} = thickness of the mucus phase diffusion layer (cm).

Applying these principles to the regional nasal uptake of the vapor of an organic acid, the following rate equations may be constructed.

Air phase.

$$V_{air}dC_{air}/dt = Q(C_{air-in} - C_{air}) - K_{gc}\,S_c(C_{air} - [X_{[nonionized]}C_{muc}/P_{muc:air}]), \quad (10)$$

where

C_{air} = concentration of the nonionized vapor exiting the air compartment under standard well-mixed compartment assumptions (i.e. $C_{air} = C_{air-out}$) ($\mu mol/cm^3$)
C_{air-in} = concentration of the nonionized vapor entering the air compartment ($\mu mol/cm^3$)
C_{muc} = total concentration of vapor in both the ionized and nonionized forms in the mucus layer ($\mu mol/cm^3$)
$X_{[nonionized]}$ = fraction of vapor present in nonionized form (dimensionless)
$P_{muc:air}$ = mucus:air partition coefficient of the nonionized acid (dimensionless) and
V_{air} = volume of air compartment (cm^3).

In some cases, the CFD simulations may indicate "leakage" of air streams between adjacent air phase compartments in the nasal cavity. In those cases, the vapor is modeled as being fully equilibrated in the upstream compartment of the CFD–PBPK model prior to transferring a fraction of the air stream to the adjacent compartment.

Mucus phase. As discussed in Appendix B of Bush *et al.* (1998), carboxylic acids are predominately ionized in viable tissues, which must maintain a pH near neutrality, and the effective diffusion rate is approximately that of the ion. The following description of the fate of absorbed vapors differs from that described by Bush *et al.* (1998) by estimating the fraction of nonionized acid in the mucus layer that is available for desorption as a function of the concentration of mucus buffer. Assuming approximately equal diffusion coefficients in the mucus and epithelium,

$$V_{muc}dC_{muc}/dt = K_{gc}S_c\,(C_{air} - (X_{[nonionized]}C_{muc}/P_{muc:air})) - D_{muc}/l_{muc-epi}S_c([(1 - X_{[nonionized]}/P_{muc:air})C_{muc}] - C_{epi1}), \quad (11)$$

where

C_{epi1} = total concentration of vapor in the epithelial layer underlying the mucus ($\mu mol/cm^3$)
$P_{epi:muc}$ = epithelial:mucus partition coefficient (dimensionless) and
$l_{muc-epi}$ = length of the diffusion path from the midpoint of mucus layer to the midpoint of the underlying epithelial layer (cm).

Ionized acids are not volatile, therefore the concentration of an acidic vapor that is available for desorption back into the air compartment is limited to the concentration of nonionized acid in the mucus. The concentration of nonionized acid is dependent on the pKa of the acid and the mucus pH. Changes in the ambient mucus pH are limited by the mucus buffer which has a finite buffering capacity (Holma, 1985). Equations 12A to 12D estimate the fraction of nonionized acid in the mucus layer, mucus pH, and the depletable mucus buffer capacity, as a function of the concentration of the vapor in the mucus. A decrease in mucus pH of approximately two units from the ambient pH is assumed to present a cytotoxic environment for the underlying epithelial cells (a nonlimiting assumption).

$$X_{[nonionized]} = 1/(1 + 10^{(pH-pKa)}) \quad (12A)$$

$$pH = (pH_i - pH_{dep}) + (1.0 - B_d)\,pH_{dep} \quad (12B)$$

$$B_d = (CB_i - CB_{muc})/CB_i \quad (12C)$$

$$V_{muc}dCB_{muc}/dt = V_{muc}(K_{muc-syn} - K_{muc-to}CB_{muc} - K_bCB_{muc}C_{muc}), \quad (12D)$$

where

pH = mucus pH
pKa = acid dissociation constant for an acidic vapor
pH_i = initial or ambient mucus pH
pH_{dep} = estimated maximum number of mucus pH units that can be depleted without significant epithelial cytotoxicity
CB_i = initial concentration of depletable mucus buffer consistent with cellular viability ($\mu mol/cm^3$).
CB_{muc} = concentration of depletable mucus buffer within a range consistent with cellular viability ($\mu mol/cm^3$).
B_d = fraction of the depletable mucus buffer capacity that has been depleted
V_{muc} = volume of mucus underlying an air compartment (cm^3)
$K_{muc-syn}$ = zero-order rate of buffer synthesis ($\mu mol/ml/h^{-1}$)
K_{muc-to} = ambient rate of buffer turnover (per h) and
K_b = estimated second-order rate of reaction of an acidic vapor with mucus buffer ($ml/h/\mu mol^{-1}$).

Epithelial phases. The description of diffusion of the vapor in the epithelial phases differs from that described by Bush *et al.* (1998) by incorporating epithelial metabolism and formally describing the migrating species as the ionized acid. For Fick's Law diffusion between adjacent tissue compartments with a partition coefficient approximately equal to unity between compartments results in:

$$V_i dC_i/dt = D_{epi}/l_{i-i-1}S_c(C_{i-i-1} - C_i) - D_{epi}/l_{i-i+1}S_c (C_i - C_{i-i+1}) - V_i K_{met} C_i\,, \quad (13)$$

where

V_i = volume of the ith tissue compartment (cm^3)
C_i, C_{i-i-1}, C_{i-i+1} = vapor concentrations in the ith tissue compartment and the compartments above and below it ($\mu mol/cm^3$)
D_{epi} = diffusivity of the compound in the epithelial phase (cm^2/h)
l_{i-i-1}, l_{i-i+1} = lengths of the diffusion paths between midpoints of epithelial layers (cm) and
K_{met} = first order rate of metabolism (h^{-1}).

Blood exchange region. Assuming approximately equal diffusion coefficients in the epithelial layer adjacent to the blood exchange region and in the blood exchange region and a partition coefficient between these regions of approximately one,

$$V_{eq} dC_{ex}/dt = D_{epi}/l_{epi-ex} S_c (C_{epi} - C_{ex}) + Q_{blood}(C_{art} - C_{ex})\,, \quad (14)$$

where

V_{ex} = volume of tissue compartment in blood exchange region (cm^3)
C_{epi} = concentration in the tissue compartment above the blood exchange region ($\mu mol/cm^3$)
C_{ex} = concentration in the blood exchange region ($\mu mol/cm^3$)
C_{art} = concentration in the arterial blood entering the blood exchange region ($\mu mol/cm^3$) and
l_{epi-ex} = length of the diffusion path from midpoint of epithelial layer adjacent to the blood exchange region to the midpoint of the blood exchange region (cm).

The species-specific parameters used in the model are listed in Table 6 for rats and humans along with the source of information for each parameter. Standard PBPK methods are used for scaling cardiac output to body weight, equilibration of blood with tissues, etc. (e.g., Frederick *et al.*, 1993). In addition, compound- and organ-specific common parameters for both models are listed below with their source.

Diffusivity of acrylic acid (ionized and nonionized) in mucus (D_{muc}) and epithelium (D_{olf} or D_{res}) was defined as 0.01 cm^2/h as an adjustable parameter from a plausible range of 0.005 to 0.02 cm^2/h based on the following considerations. A lower limit value of 0.005 cm^2/h was calculated for the diffusion coefficient of acrylic acid in water (Bush *et al.*, 1998) corrected for the increased bulk viscosity of mucus and tissue relative to water. A value of approximately 0.015 cm^2/h was measured experimentally for similar sized charged ions and neutral molecules by Kushmerick and Podolsky (1969) in muscle fibers. Generally, experimentally determined diffusion coefficients of similarly sized molecules in tissue are approximately 0.3 to 0.5 the values determined in water (Kushmerick and Podolsky, 1969; George *et al.*, 1996). The experimentally determined diffusion coefficient of the closely related compound, propionic acid, in water is 0.038 cm^2/h (Cussler, 1997, p. 112), therefore the predicted value in tissue would be in the 0.01 to 0.02 cm^2/h range. Final selection of 0.01 from the plausible range was based on fitting the predictions of the model for whole-nose uptake to the unidirectional uptake date for a slowly metabolized vapor with approximately the same molecular weight as acrylic acid (acetone at a flow rate of 100 ml/min; Fig. 6). Interestingly, this value gave a good fit to the model predictions to the whole-nose uptake of a wide variety of slowly metabolized vapors that span a wide molecular weight range (Fig. 6). As noted by Bush *et al.* (1998) the hybrid CFD–PBPK model predictions of overall uptake of inhaled vapors in the rat nasal cavity are sensitive to variations in the value of D_{muc}.

Diffusivity of acrylic acid in squamous epithelium of the nasal vestibule equals 0.001 cm^2/h based upon estimates of the diffusivity of small organic molecules across dermal tissue (Environmental Protection Agency, 1992).

Thickness of mucus layer is 10 μm in all regions (Morgan *et al.*, 1984 and personal communication), except that the mucus covering the human olfactory epithelium is 20-μm thick (Lang, 1989, p. 119).

Based upon photomicrographs of rat nasal tissues and a micrometer, the approximate thicknesses of the epithelial layers are as follows: respiratory and squamous epithelia = 25 μm, the blood exchange regions under the respiratory and squamous epithelia = 75 μm, the olfactory epithelium = 80 μm, and the blood exchange region under the olfactory epithelium = 50 μm.

Partition coefficients for acrylic acid between compartments were as follows:

Lung:blood = 1.4 (Black and Finch, 1995)
Liver:blood = 1.7 (Black and Finch, 1995)
Muscle/Fat:blood = 1.2 (Black and Finch, 1995)
Other perfused:
blood = 1.4 (Black and Finch, 1995)

Nasal
epithelium:blood = 1.4 (Assumed to be similar to lung:blood)
Blood:air = 6100 (Table 3 [pH 2.0 to suppress ionization])
Mucus:air = 1780 (Table 3 [similar to saline at pH 2.0 to suppress ionization of the weak acid])
Nasal
epithelium:mucus = 1.0 (Based on micropartitioning studies of Black and Finch [1995]; assumed to primarily reflect partitioning of the ionized acid)

Ambient mucus pH = 6.6 (Boden *et al.*, 1983) with a buffer capacity such that 6 μmol of acid will deplete 1 ml of mucus 1 pH unit (Holma, 1985). A mucus pH of less than 4.6 is assumed to cause epithelial cytotoxicity. Rate of mucus secretion = 0.21 ml/h/cm^2 (Hatch, 1992). pKa of acrylic acid = 4.25. Estimated second order rate of reaction of an acidic vapor with mucus buffer = 300 ml/h/μmol.

Pseudo first-order rate of metabolism of acrylic acid in liver = 4.2 h^{-1} and all other tissues = 0.7 h^{-1} (Black and Finch, 1995).

ACKNOWLEDGMENTS

Technical support for these studies by Mr. John Udinsky is gratefully acknowledged. Dr. Melvin Andersen (ICF Kaiser) provided thoughtful comparisons between the nasal deposition of vapors from inhaled air and the pharmacokinetic clearance of compounds from the systemic circulation by tissues. Dr. Peter W. Scherer and his students (University of Pennsylvania) provided valuable technical insight in modeling air flow in the human nasal cavity. These studies were supported by the Basic Acrylic Monomer Manufacturers and Rohm and Haas Company.

REFERENCES

Black, K. A., and Finch, L. (1995). Acrylic acid oxidation and tissue-to-blood partition coefficients in rat tissues. *Toxicol. Lett.* **78,** 73–78.

Bodem, C. R., Lampton, L. M., Miller, P., Tarka, E. F., and Everett, E. D. (1983). Endobronchial pH. *Am. Rev. Respir. Dis.* **127,** 39–41.

Brass, E. P. (1994). Overview of coenzyme A metabolism and its role in cellular toxicity. *Chem.–Biol. Interact.* **90,** 203–214.

Bush, M. L., Frederick, C. B., Kimbell, J. S., and Ultman, J. S. (1998). A CFD–PBPK hybrid model for simulating gas and vapor uptake in the rat nose. *Toxicol. Appl. Pharmacol.* **150,** 133–145.

Cussler, E. L. (1997). *Diffusion: Mass Transfer in Fluid Systems,* 2nd ed., pp. 101–244. Cambridge University Press, Cambridge.

Custodio, J. B. A., Palmeira, C. M., Moreno, A. J., and Wallace, K. B. (1998). Acrylic acid induces the glutathione-independent mitochondrial permeability transition in vitro. *Toxicol. Sci.* **43,** 19–27.

Delp, M. D., Manning, R. O., Bruckner, J. V., and Armstrong, R. B. (1991). Distribution of cardiac output during diurnal changes of activity in rats. *Am. J. Physiol.* **261,** H1487–H1493.

DeSesso, J. M. (1993). The relevance to humans of animal models for inhalation studies of cancer in the nose and upper airways. *Quality Assurance: Good Practice, Regulation, and Law* **2,** 213–231.

Dorato, M. A., Carlson, K. H., and Copple, D. L. (1983). Pulmonary mechanics in conscious Fischer 344 rats: Multiple evaluations using nonsurgical techniques. *Toxicol. Appl. Pharmacol.* **68,** 344–353.

Environmental Protection Agency (1992). *Dermal Exposure Assessment: Principles and Applications,* pp. 4.10, 5.34. EPA/600/8-91/011B, Office of Research and Development, Washington, D.C.

Environmental Protection Agency (1994). *Methods for Derivation of Inhalation Reference Concentrations and Application of Inhalation Dosimetry,* pp. 4.28–4.29. EPA/600/8-90/066F, Office of Research and Development, Washington, D.C.

Frederick, C. B., Morris, J. B., Kimbell, J. S., Morgan, K. T., and Scherer, P. T. (1994). Comparison of four biologically based dosimetry models for the deposition of rapidly metabolized vapors in the rodent nasal cavity. *Inhal. Toxicol.* **6**(Suppl.), 135–157.

Frederick, C. B., Potter, D. W., Chang-Mateu, M. I., and Andersen, M. E. (1992). A physiologically based pharmacokinetic and pharmacodynamic model to describe oral dosing of rats with ethyl acrylate and its implications for risk assessment. *Toxicol. Appl. Pharmacol.* **114,** 246–260.

Gargas, M. L., Burgess, R. J., Voisard, D. E., Cason, G. H., and Andersen, M. E. (1989). Partition coefficients of low molecular weight volatile chemicals in various liquids and tissues. *Toxicol. Appl. Pharmacol.* **98,** 87–99.

Gerde, P., and Dahl, A. R. (1991). A model for the uptake of inhaled vapors in the nose of the dog during cyclic breathing. *Toxicol. Appl. Pharmacol.* **109,** 276–288.

George, S. C., Babb, A. L., Deffebach, M. E., and Hlastala, M. P. (1996). Diffusion of nonelectrolytes in the canine trachea: Effect of tight junction. *J. Appl. Physiol.* **80,** 1687–1695.

Godo, M. N., Morgan, K. T., Richardson, R. B., and Kimbell, J. S. (1995). Reconstruction of complex passageways for simulations of transport phenomena: Development of graphical user interface for biological applications. *Comp. Meth. Prog. Biomed.* **47,** 97–112.

Gross, E. A., and Morgan, K. T. (1992). Architecture of nasal passages and larynx. In *Comprehensive Treatise on Pulmonary Toxicology.* Volume I. *Comparative Biology of the Normal Lung* (R. A. Parent, Ed.), pp. 7–25. CRC Press, Boca Raton, FL.

Gross, E. A., Swenberg, J. A., Fields, S., and Popp, J. A. (1982). Comparative morphometry of the nasal cavity in rats and mice. *J. Anat.* **135,** 83–88.

Hahn, I., Scherer, P. W., and Mozell, M. M. (1993). Velocity profiles measured for air flow through a large-scale model of the human nasal cavity. *J. Appl. Physiol.* **75,** 2273–2287.

Hanna, L. M., Frank, R., and Scherer, P. W. (1989). Absorption of soluble gases and vapors in the respiratory system. In *Respiratory Physiology* (H. K. Chang and M. Paiva, Eds.), pp. 277–316. Marcel-Dekker, New York.

Hatch, G. E. (1992). Comparative biochemistry of airway lining fluid. In *Comparative Biology of the Normal Lung* (R. A. Parent, Ed.), pp. 617–632. CRC Press, Boca Raton, FL.

Holma, B. (1985). Influence of buffer capacity and pH-dependent rheological properties of respiratory mucus on health effects due to acidic pollution. *Sci. Total Environ.* **41,** 101–123.

International Commission of Radiological Protection (ICRP) (1975). No. 23: *Report of the Task Group on Reference Man,* pp. 235–237, 346. Pergamon Press, New York.

Keenan, C. M., Kelly, D. P., and Bogdanffy, M. S. (1990). Degeneration and recovery of rat olfactory epithelium following inhalation of dibasic esters. *Fundam. Appl. Toxicol.* **15,** 381–393.

Keyhani, K., Scherer, P. W., and Mozell, M. M. (1995). Numerical simulation of airflow in the human nasal cavity. *J. Biomed. Engr.* **117,** 429–442.

Kimbell, J. S., Gross, E. A., Joyner, D. R., Godo, M. N., and Morgan, K. T. (1993). Application of computational fluid dynamics to regional dosimetry

of inhaled chemicals in the upper respiratory tract of the rat. *Toxicol. Appl. Pharmacol.* **121,** 253–263.

Kimbell, J. S., Gross, E. A., Richardson, R. B., Conolly, R. B., and Morgan, K. T. (1997). Correlation of regional formaldehyde flux predictions with the distribution of formaldehyde-induced squamous metaplasia in F344 rat nasal passages. *Mutat. Res.* **380,** 143–154.

Kushmerick, M. J., and Podolsky, R. J. (1969). Ionic mobility in muscle cells. *Science (Washington, D.C.)* **166,** 1297–1298.

Lang, J. (1989). *Clinical Anatomy of the Nose, Nasal Cavity, and Paranasal Sinuses.* pp. 42–45, 112–119. Thieme, Stuttgart.

Lee, K.-P., Valentine, R., and Bogdanffy, M. S. (1992). Nasal lesion development and reversibility in rats exposed to aerosols of dibasic esters. *Toxicol. Pathol.* **20,** 376–393.

Lomax, L. G., Brown, D. W., and Frederick, C. B. (1994). Regional histopathology of the mouse nasal cavity following two weeks of exposure to acrylic acid for either 6 or 22 hours per day. *Inhal. Toxicol.* **6**(Suppl.), 445–449.

Lyman, W. J., Reehl, W. F., and Rosenblatt, D. H. (1990). *Handbook of Chemical Property Estimation Methods: Environmental Behavior of Organic Compounds.* pp. 15.9–15.32. American Chemical Society, Washington, D.C.

Mery, S., Gross, E. A., Joyner, D. R., Godo, M., and Morgan, K. T. (1994). Nasal diagrams: A tool for recording the distribution of nasal lesions in rats and mice. *Toxicol. Pathol.* **22,** 353–372.

Miller, F. J., Overton, J. H., Kimbell, J. S., and Russell, M. L. (1993). Regional respiratory tract absorption of inhaled reactive gases. In *Toxicology of the Lung,* 2nd. ed. (D. E. Gardner, J. D. Crapo, and R. O. McClellan, Eds.), pp. 485–525. Raven Press, New York.

Miller, R. R., Ayres, J. A., Jersey, G. C., and McKenna, M. J. (1981). Inhalation toxicity of acrylic acid. *Fundam. Appl. Toxicol.* **1,** 271–277.

Miller, R. R., Letts, R. L., Potts, W. J., and McKenna, M. J. (1980). Improved methodology for generating controlled test atmospheres. *Am. Ind. Hyg. Assoc. J.* **41,** 271–277.

Miller, R. R., Young, J. T., Kociba, R. J., Keyes, D. G., Bodner, K. M., Calhoun, L.L., and Ayres, J. A. (1985). Chronic toxicity and oncogenicity bioassay of inhaled ethyl acrylate in Fischer 344 rats and B6C3F1 mice. *Drug Chem. Toxicol.* **8,** 1–42.

Morgan, K. T., Jiang, X.-Z., Patterson, D. L., and Gross, E. A. (1984). The nasal mucociliary apparatus. *Am. Rev. Respir. Dis.* **130,** 275–281.

Morgan, K. T., Kimbell, J. S., Monticello, T. M., Patra, A. L., and Fleishman, A. (1991). Studies of inspiratory airflow patterns in the nasal passages of the F344 rat and rhesus monkey using nasal molds: Relevance to formaldehyde toxicity. *Toxicol. Appl. Pharmacol.* **110,** 223–240.

Morgan, K. T., and Monticello, T. M. (1990). Airflow, gas deposition, and lesion distribution in the nasal passages. *Environ. Health Perspect.* **85,** 209–218.

Morris, J. B. (1991). Deposition of acetone vapor in the upper respiratory tract of the B6C3F1 mouse. *Toxicol. Lett.* **56,** 187–196.

Morris, J. B., and Frederick, C. B. (1994). Upper respiratory tract uptake of acrylate ester and acid vapors. *Inhal. Toxicol.* **7,** 557–574.

Morris, J. B., Hassett, D. N., and Blanchard, K. T. (1993). A physiologically based pharmacokinetic model for nasal uptake and metabolism of nonreactive vapors. *Toxicol. Appl. Pharmacol.* **123,** 120–129.

Morris, J. B., and Smith, F. A. (1982). Regional deposition and absorption of inhaled hydrogen fluoride in the rat. *Toxicol. Appl. Pharmacol.* **62,** 81–89.

Nakashima, T., Kimmelman, C. P., and Snow, J. B. (1984). Structure of human fetal and adult olfactory neuroepithelium. *Arch. Otolaryngol.* **110,** 641–646.

Nakashima, T., Tanaka, M., Inamitsu, M., and Uemura, T. (1991). Immunohistopathology of variations of human olfactory mucosa. *Eur. Arch. Oto-Rhino-Laryngol.* **248,** 370–375.

National Toxicology Program (1992). NTP technical report on toxicity studies of formic acid administered by inhalation for F344/N rats and B6C3F1 mice. NIH Publication 92-3342.

Reininghaus, W., Koestner, A., and Klimisch, H.-K. (1991). Chronic toxicity and oncogenicity bioassay of inhaled methyl acrylate and *n*-butyl acrylate in Sprague–Dawley rats. *Food Chem. Toxicol.* **29,** 329–339.

Sherrat, H. S. A. (1985). Acyl-CoA esters of xenobiotic carboxylic acids as biochemically active intermediates. *Biochem. Soc. Trans.* **13,** 856–858.

Stott, W. T., Ramsey, J. C., and McKenna, M. J. (1986). Absorption of chemical vapors by the upper respiratory tract of rats. In *Toxicology of the Nasal Passages* (C. S. Barrow, Ed.), pp. 191–210. Hemisphere, Washington, D.C.

Subramaniam, R., Richardson, R. B., Morgan, K. T., Kepler, G., Kimbell, J. S., and Guilmette, R. A. (1998). Computational fluid dynamics simulations of inspiratory airflow in the human nose and nasopharynx. *Inhal. Toxicol.* **10,** 91–120.

Swift, D. L., and Proctor, D. F. (1977). Access of air to the respiratory tract. In *Respiratory Defense Mechanisms* (J. D. Brain, D. F. Proctor, and L. M. Reid, Eds.), pp. 63–93. Marcel Dekker, New York.

Talamo, B. R., Feng, W.-H., and Stockmayer, M. (1995). Human olfactory epithelium: Normal patterns and types of lesions found in the general population. *Inhal. Toxicol.* **6**(Suppl.), 249–275.

Trela, B. A., and Bogdanffy, M. S. (1991). Cytotoxicity of dibasic esters (DBE) metabolites in rat nasal explants. *Toxicol. Appl. Pharmacol.* **110,** 259–267.

Trela, B. A., Frame, S. R., and Bogdanffy, M. S. (1992). A microscopic and ultrastructural evaluation of dibasic esters (DBE) toxicity in rat nasal explants. *Exp. Mol. Pathol.* **56,** 208–218.

Uraih, L. C., and Maronpot, R. R. (1990). Normal histology of the nasal cavity and application of special techniques. *Environ. Health Perspect.* **85,** 187–208.

Williams, L. R., and Leggett, R. W. (1989). Reference values for resting blood flow to organs of man. *Clin. Phys. Meas.* **10,** 187–217.